Center for Environmentally Sustainable Transportation in Cold Climates

Pre-Stress Loss due to Creep in Precast Concrete Decked Bulb-Tee Girders under Cold Climate Conditions

Drew Vandermeer and Il-Sang Ahn, Ph.D., P.E.
Department of Civil and Environmental Engineering
University of Alaska Fairbanks

Date: 7/31/2019

Prepared by: Il-Sang Ahn and Drew Vandermeer

Center for Environmentally Sustainable Transportation in Cold Climates
University of Alaska Fairbanks
P.O. Box 755900
Fairbanks, AK 99775

U.S. Department of Transportation
1200 New Jersey Avenue, SE
Washington, DC 20590

INE/CESTiCC 19.14

REPORT DOCUMENTATION PAGE

Form approved OMB No.

1. AGENCY USE ONLY (LEAVE BLANK)	2. REPORT DATE	3. REPORT TYPE AND DATES COVERED
	7/2019	Final Report: 09/2016 – 12/2018

4. TITLE AND SUBTITLE

Prestress Loss due to Creep in Precast Concrete Decked Bulb-Tee Girders in Cold Climates

5. FUNDING NUMBERS

6. AUTHOR(S)

Drew Vandermeer, Graduate Research Assistant
Il-Sang Ahn, Ph.D., P.E.
University of Alaska Fairbanks

7. PERFORMING ORGANIZATION NAME(S) AND ADDRESS(ES)

Center for Environmentally Sustainable Transportation in Cold Climates
University of Alaska Fairbanks
Duckering Building, Room 245
P.O. Box 755900
Fairbanks, AK 99775-5900

8. PERFORMING ORGANIZATION REPORT NUMBER

INE/CESTiCC 19.14

9. SPONSORING/MONITORING AGENCY NAME(S) AND ADDRESS(ES)

10. SPONSORING/MONITORING AGENCY REPORT NUMBER

11. SUPPLENMENTARY NOTES

12a. DISTRIBUTION / AVAILABILITY STATEMENT

No restrictions

12b. DISTRIBUTION CODE

13. ABSTRACT (Maximum 200 words)

Accurate estimation of pre-stress losses is one of the important issues for the design of precast, pre-stressed concrete bridge girders. While this subject has been long studied by many researchers, studies on pre-stress losses in cold climates are minimal. In the present research, long-term pre-stress loss due to concrete creep was studied based on concrete creep test. Two concrete creep test frames were fabricated and placed indoors and outdoors. Concrete strains were measured by Demountable Mechanical Strain Gauge (DEMEC) from two 6″×12″ high-strength concrete cylinders in each frame. The concrete strains were collected for 11 months (7/26/2017 – 6/21/2018) after loading, and outdoor ambient temperature dropped below 0°C between 100 and 250 days. Between 50 and 100 days, two curves from the two frames are similar in their patterns and values. After 100 days, the total strain from the indoor frame slowly increased reaching 1,600 and 1,700με after 250 days. However, the total strain from the outdoor frame varied between 1,000 and 1,500με and the averaged total strain was 1,300με after 250 days. In cold temperature, the occurrence of concrete creep and shrinkage was suppressed.

14- KEYWORDS : Cold Temperature, Pre-stress Losses, Concrete Creep, Concrete Shrinkage, AASHTO, Creep Frame

15. NUMBER OF PAGES

95

16. PRICE CODE

N/A

17. SECURITY CLASSIFICATION OF REPORT	18. SECURITY CLASSIFICATION OF THIS PAGE	19. SECURITY CLASSIFICATION OF ABSTRACT	20. LIMITATION OF ABSTRACT
Unclassified	Unclassified	Unclassified	N/A

ACKNOWLEDGEMENTS

The research reported herein was performed by the Department of Civil and Environmental Engineering, University of Alaska Fairbanks. Dr. Il-Sang Ahn, Assistant Professor, was the principal investigator. Drew Vandermeer, a graduate student in the Department of Civil and Environmental Engineering, co-authored this report. The research was conducted under the general supervision of Dr. Ahn. The groups that have been a big help in the development of this report are as follows: AggPro for product management, Alaska Department of Transportation Northern Regional Lab with assistance in storage and strength tests, Jon's Machine Shop for frame manufacturing, and CESTiCC for their financial support.

TABLE OF CONTENTS

LIST OF FIGURES

LIST OF TABLES

EXECUTIVE SUMMARY

Accurate estimation of pre-stress losses is an important issue when designing precast, pre-stressed concrete bridge girders. While many researchers have studied pre-stress losses, studies on pre-stress losses in cold climates are rare. The project conducted concrete creep tests to study long-term pre-stress loss due to concrete creep. Two concrete creep test frames were built, with one placed indoors and one placed outdoors. Concrete strains were measured by Demountable Mechanical Strain Gauges (DEMEC) from two 6″×12″ high-strength concrete cylinders in each frame and were collected for 11 months (7/26/2017 – 6/21/2018) after loading. The outdoor ambient temperature dropped below 0°C between 100 and 250 days after measurement started.

Between 0 and 50 days after measurement started, the total strains from the outdoor frame were considerably bigger than the ones from the indoor frame. Between 50 and 100 days after measurement started, total strains from the two frames were similar in their patterns and values. After 100 days, the total strain from the indoor frame slowly increased reaching between 1,600 and 1,700 $\mu\varepsilon$ after 250 days. However, the total strain from the outdoor frame varied between 1,000 and 1,500 $\mu\varepsilon$ and the averaged total strain was 1,300 $\mu\varepsilon$ after 250 days. The shrinkage strain from indoor specimens showed a change of roughly 500$\mu\varepsilon$ in the first 50 days, and then a steadily increasing trend went on until measurement stopped. The outdoor specimens showed a similar trend within the first 50 days at roughly 500$\mu\varepsilon$. Between 150 and 250 days after measurement started, the strain did not change much compared to the indoor specimens. Cold temperatures suppressed the occurrence of concrete creep and shrinkage. Therefore, pre-

stress losses due to concrete creep and shrinkage can occur for a longer period in the cold climate.

CHAPTER. 1 INTRODUCTION

1.1 Research Need

The popularity of using high-strength concrete for bridges has increased in recent years among many state highway agencies, such as Departments of Transportation and the Federal Highway Administration (FHWA). As of 2014, 44% of Alaska's state and local bridge inventory is concrete, but concrete bridges account for approximately 80% of the new bridges built by the Alaska Department of Transportation & Public Facilities (ADOT&PF) **(**Daugherty and Marx 2014**)**. The concrete bridge provides economic benefits through increased girder spacing, length, and lifespan. Due to its excellent adaptability to the constraints in Alaska, the Decked Bulb-Tee (DBT) girder is the most common type of bridge superstructure used by ADOT&PF. The DBT girder is a precast, pre-stressed concrete bulb-tee girder with a deck cast monolithically and pre-stressed with the girder (Oesterle et al. 2009, PCI 2011). Figure 1-1 shows the standard cross-section of Alaska-style DBT girders, where the deck width can reach 8.5 feet (ADOT&PF 2017).

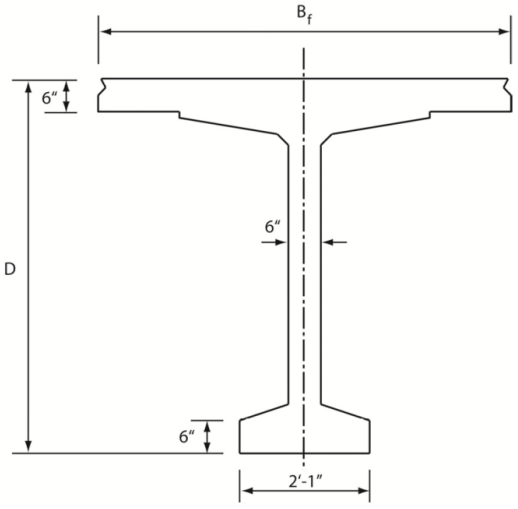

Figure 1-1. Standard Alaska-Style Precast DBT Girder Section (ADOT&PF 2017)

The long-term durability and wear-resistance of DBT girders to the Alaskan environment have proven to be outstanding. During the last ten years, approximately 80% of the new bridges constructed in Alaska have been DBT girders. There has been almost no girder-related maintenance required on the 273 bridges of this style built in Alaska since 1973 **(**Daugherty and Marx 2014**)**.

A DBT girder utilizes pre-stressing force applied to the girder by pre-stressing strands inside the girder during the fabrication. The pre-stressing force lets a DBT girder span a long distance. The amount of pre-stressing force in the girder ensures the serviceability and safety of the bridge. However, the pre-stressing force initially applied during fabrication of a DBT girder decreases. The amount of force decreased, known as "pre-stress loss," occurs through several mechanisms when the bridge is both under construction and in service.

While pre-stress losses have been active research topic, studies for pre-stress losses in the design of pre-stressed concrete girders in cold climates are minimal. Therefore, additional research is required to provide information to understand cold climate effects.

In Alaska, long-term pre-stress losses are different from other states due to:

- Different aggregate : the influence of different aggregate on the elastic modulus and creep coefficient of concrete was noted in Tadros et al. (2003).
- Fewer DBT girder fabricators in Alaska; there have been only three fabricators, with most of the work performed by one fabricator in Anchorage so the material quality and workmanship can be relatively uniform among girders.

- Shorter time between fabrication and placement of girders, typically the time in a storage yard is 60 days[1] in Alaska. Storage time is much longer in other states.
- Cold climates and extreme annual temperature variation in Alaska.

1.2 Objective and Scope of the Study

The goal of this research is to develop more accurate design parameters for estimating pre-stress losses in DBT girders due to concrete creep in cold climates. In the design of DBT girders, the amount of pre-stress force determines short-term and long-term stresses in concrete. If the pre-stress loss is underestimated, the concrete stress at the bottom of a girder at midspan may experience the tensile stresses that exceed the tensile strength of concrete, which can compromise the durability and long-term performance of the girder. If the pre-stress loss is overestimated, however, more pre-stressing strands will be required than are necessary, which may increase the cost of girder fabrication, reduce the maximum span length, or increase the number of girders. The accurate estimation of pre-stress losses, therefore, is important in the design process.

Pre-stress losses can dramatically vary depending on a girder's thermal environment, which directly affects its curing process. However, it is hard to find research focused on DBT girders despite extensive pre-stress loss research. Specifically, in-situ measurement of pre-stress loss data for DBT girders over a long period is extremely rare or does not exist. As the major

[1] From a DBT girder fabricator in AggPro in Anchorage, AK. Time to placement ranges from two weeks after casting to siting in storage through the winter.

portion of time-dependent pre-stress losses is due to concrete creep, this research focused on this specific mechanism.

The objectives of the present research are:

1. Acquiring a better understanding of concrete creep in cold climate regions. Since concrete creep depends on concrete mix design and environmental conditions, the project conducted a physical concrete creep test in ambient environment of cold climate to evaluate concrete creep. The study contained two identical concrete creep test setups; one outdoors in the natural Alaskan environment, while the second is in a lab indoors with controlled conditions.
2. Understanding specific design issues for DBT girders related to time-dependent pre-stress losses. The difference in design and construction between DBT girders and conventional pre-stressed girders should be well understood, since the majority of existing pre-stress loss provisions have been developed for conventional pre-stressed girders.
3. Within the framework of current provisions in the *AASHTO LRFD Bridge Design Specifications* (AASHTO 2017), the project compared pre-stress losses due to concrete creep and shrinkage.

CHAPTER. 2 LITERATURE REVIEW

2.1 Background

Over the past 20 years, the use of precast modular components to accelerate bridge construction has increasingly gained attention in the United States. Precast concrete components are transported separately and assembled at the construction site, minimizing cast-in-place concrete work at the site. Since the time occupying the construction site can be substantially reduced, precast modular construction allows bridge engineers to minimize accidents in the work zone, reduce traffic disruptions, and increase the speed of construction, while maintaining construction quality, and minimizing the lifetime costs and environmental impact (Shahawy 2003, PCINE 2014). The Linn Cove Viaduct in North Carolina (Figg and Pate 2004) and the Getty Museum People-Mover Guideway in California (Josten et al. 1995) provide examples of projects that used precast concrete components to minimize environmental impact during the construction of substructures. In cold climate regions, accelerated bridge construction (ABC) is a particularly important strategy due to the short construction season (ADOT&PF 2017).

The environment where concrete cures is an important factor that controls the mechanical properties of the concrete. Just after the completion of construction, exposure of concrete bridges in cold climate regions to severely cold weather occurs in the winter. Figure 2-1 shows daily average temperature and ambient relative humidity of several cities in cold climate regions (ClimaTemps 2016; Current Results Nexus 2016a; Wikipedia 2016a, 2016b). The average winter (December – February) temperature is -6.7 °F in Fairbanks, AK, 29.4 °F in Spokane, WA, and 22.4 °F in Helena, MT. For the entire U.S., excluding Hawaii and Alaska, the average winter temperature is 33.2 °F (Current Results Nexus 2016b).

The ambient relative humidity has a significant influence on concrete creep (Park and Paulay 1975). Creep strains are low when the relative humidity is high, because creep is reduced if water loss from the member is restricted. During a typical construction season (June – October), the average relative humidity is 58.2% in Fairbanks, AK, 52.7% in Spokane, WA, and 51.8% in Helena, MT. In the AASHTO LRFD Bridge Design Specifications (AASHTO LRFD), the average annual ambient relative humidity in Fairbanks and Spokane is greater than 70% (AASHTO 2017). The concrete creep strains in such regions could be different from those anticipated in AASHTO LRFD.

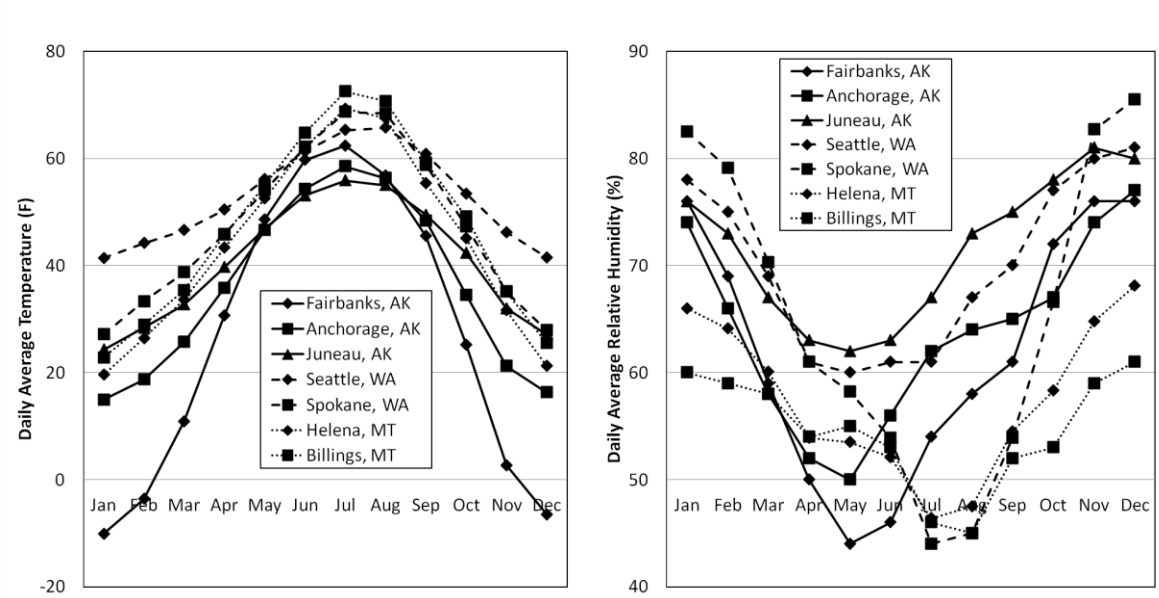

Figure 2-1. Daily Average Temperature and Daily Average Relative Humidity of Several Cities in Cold Climate Regions

The total pre-stress loss separates into two groups: (1) instantaneous losses and (2) long-term time-dependent losses (AASHTO 2017). Losses due to anchorage set, friction, and elastic shortening group as an instantaneous loss; losses due to concrete creep, concrete shrinkage, and

relaxation of pre-stressing strands classify as time-dependent losses. Figure 2-2 demonstrates the change in pre-stress force that occurs during bridge construction activities.

- A – C: Pre-stress loss due to pre-stressing bed anchorage seating, relaxation between initial tensioning and transfer, and temperature change in strand embedded in concrete. The losses from the bed anchorage seating (A – B) are not present in either pre-stressing strands or concrete.
- C – D: Instantaneous pre-stress loss at transfer due to elastic deformation and self-weight.
- D – E and F – G: Time-dependent pre-stress loss due to shrinkage and creep of girder concrete and relaxation of pre-stressing strands.
- E – F: Increasing tensile stress due to superimposed dead loads (SIDL).

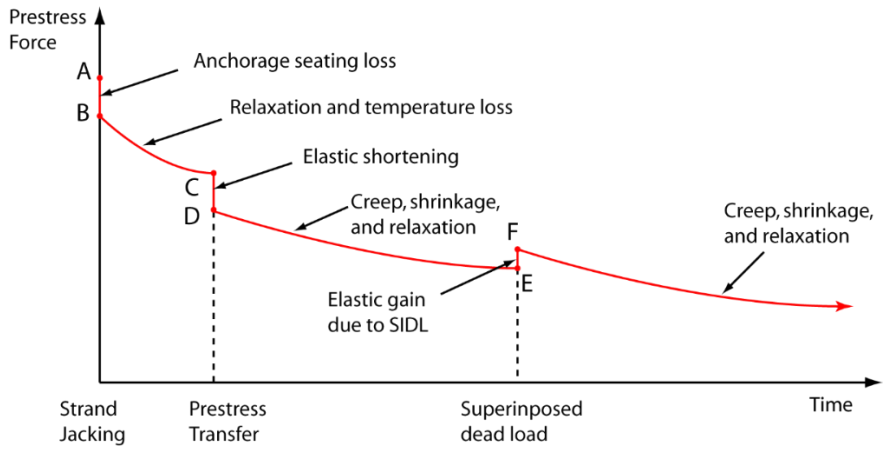

Figure 2-2. Pre-stressing Strand Force Changes with Time [modified from (Tadros et al. 2003) to represent DBT girders]

At transfer, compressive stresses are imposed to the concrete. In the current AASHTO LRFD (AASHTO 2017), the maximum allowable compressive stress at pre-stress transfer is

$0.65 f_{ci}^{'}$, where, $f_{ci}^{'}$ is concrete strength at transfer[2]. Figure 2-3 shows corresponding compressive stress changes at the bottom fiber concrete (tension side when subject to gravity loads) of a girder. When placing superimposed dead loads (SIDL), tensile stress increases both in the pre-stressing strands and in the concrete. This induces stress "gain" in the pre-stressing strands (see Figure 2-2) and additional tensile stress at the bottom of the girder (see Figure 2-3). The tension side of the girder experiences only an increase in tensile stress and pre-stress "gains" do not equate to a reduction in pre-stress losses over time.

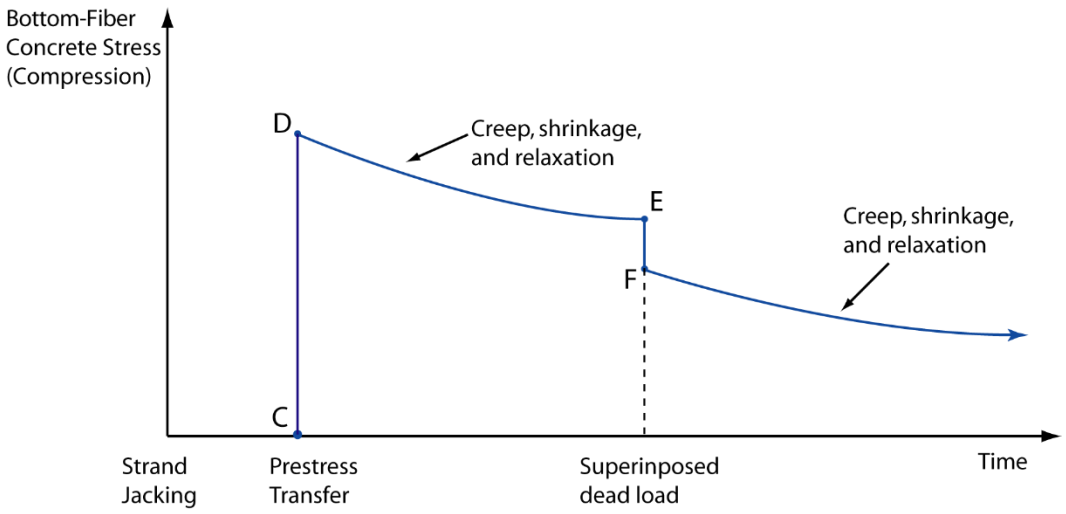

Figure 2-3. Bottom-Fiber Compressive Stress Changes [modified from Garber et al. (2013) to represent DBT girders]

Concrete shrinkage, concrete creep, and relaxation of pre-stressing strands are three major mechanisms contributing to time-dependent pre-stress losses. Among them, pre-stress loss due to creep is the most significant. For instance, the percentages of pre-stress losses due to

[2] This revision was made in 2016 Interim

creep, shrinkage, and relaxation to the total time-dependent losses were 68%, 24%, and 8%, respectively, for two example bridges in Tadros et al. (2003) and Roller et al. (2011). Due to creep, concrete strain under a constant stress increases with time. This occurs because the elastic modulus of the concrete under a constant stress decreases with the rate of loading.

Figure 2-4 shows the concrete stress-strain relationships that depend on the rate of loading (Rüsch 1960). When hardened concrete cylinders were loaded with a slow rate of loading (longer than 1 hour), the strength of concrete decreased compared to the strength observed from a loading occurring in minutes, which is typical for a concrete cylinder test. Collins and Mitchell (1997) reported that the strength reduction was about 20% of the 28-day strength. Concrete typically gains 20 to 40% in strength due to continuing hydration. These two phenomena compensate for each other, resulting in a conservative assumption on the 28-day concrete strength, so the strength reduction caused by long-term loading was not considered in the design (Collins and Mitchell 1997).

Figure 2-5 demonstrates concrete creep in stress-strain relationships (Rüsch 1960). When applying a stress to a concrete cylinder at a rate of $t = 20\,\text{min}.$ and the rate held constant for a long time, the strain increases as the stress-strain relationship changes with time. Theoretically, the creep stops as the strain reaches the creep limit, a stress-strain relationship for a load with a rate of $t = \infty.$ For estimating concrete creep, therefore, the stress-strain relationship of concrete at different ages and under different stress histories should be known.

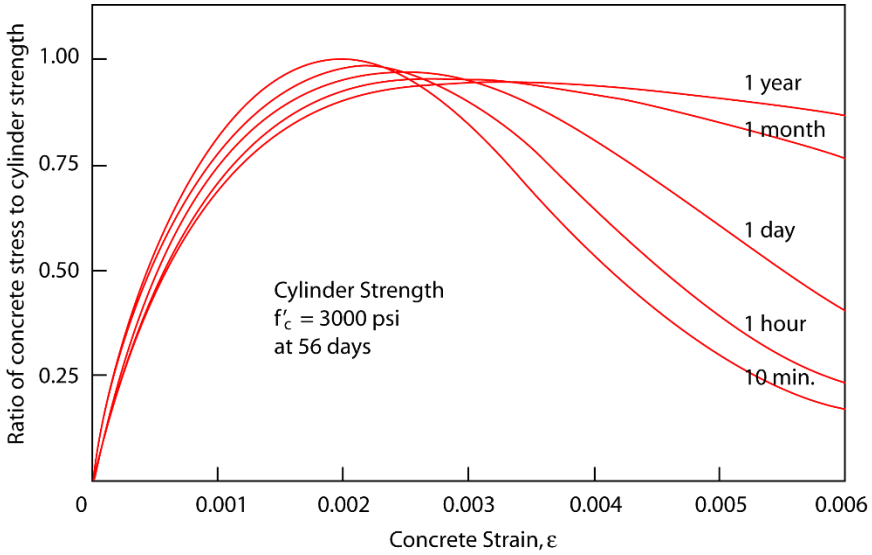

Figure 2-4. Stress-Strain Relationships for Eccentric Compression after Various Durations of Loading at Constant Strain Rates (Rüsch 1960)

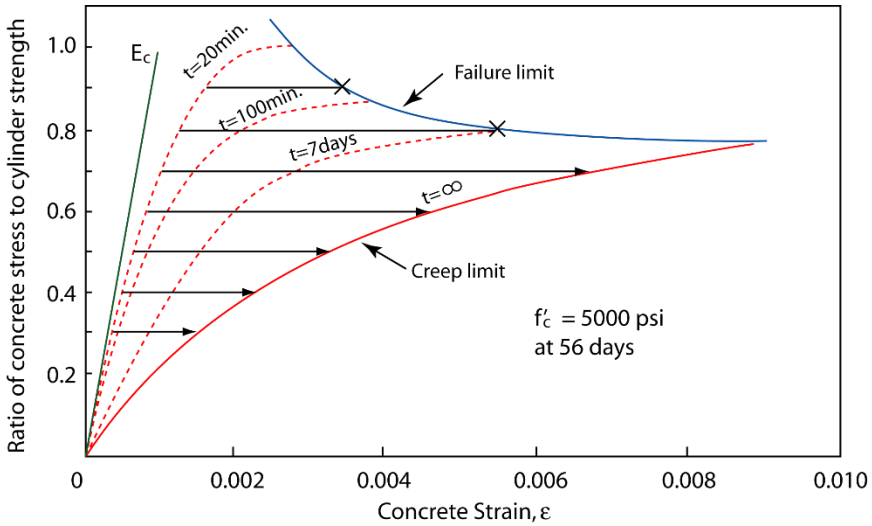

Figure 2-5. Influence of Load Intensity and Duration on Concrete Strain (Rüsch 1960)

Figure 2-6 illustrates the creep deformation of concrete with time under constant axial compressive stress (Park and Paulay 1975). The creep would proceed at a decreasing rate with

time. Remove the load, the elastic strain immediately recovers. However, the elastic recovery is less than the initial elastic strain, because the elastic modulus of concrete increases with age[3]. The creep strain occurring over a given time is proportional to the applied stress if the stress level is not high. Concrete creep strain is the permanent strain that remains in the concrete that was loaded for some time and unloaded. For the usual range of concrete stress used in structural design, the assumption of a linear relationship between creep strain and applied stress is acceptable.

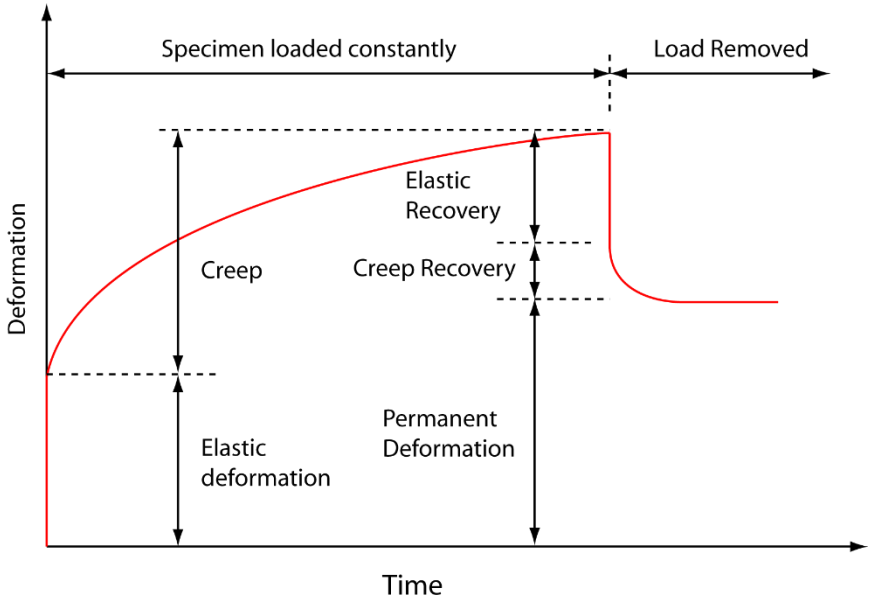

Figure 2-6. Typical Creep Curve with Constant Axial Compressive Stress (Park and Paulay 1975)

[3] After the start of concrete hardening, the stress-strain relationship under short-term loading is different from the stress-strain relationship under long-term loading for the same concrete.

The stress-strain relationship of concrete can be represented by various models, and a linear elastic relationship in Equation 2-1 can be used if the stress is low, $f_c < 0.6 f_c^{'}$ (Collins and Mitchell 1997).

$$f_c = E_c \varepsilon_{cf} \tag{2-1}$$

where

f_c = the concrete stress

$f_c^{'}$ = the maximum stress (strength),

ε_{cf} = the concrete strain caused by f_c

E_c = the tangent modulus when $\varepsilon_{cf} = 0$.

AASHTO LRFD (AASHTO 2017) uses Equation 2-2 for the estimation of E_c.

$$E_c = 120,000 K_1 w_c^{2.0} \left(f_c^{'} \right)^{0.33} \qquad (ksi) \tag{2-2}$$

where

K_1 = correction factor for source of aggregate

w_c = unit weight of concrete (kcf)

The difference between this secant modulus and the tangent modulus is negligible for the concrete used in typical pre-stressed concrete (Collins and Mitchell 1997). The total concrete strain due to a sustained stress $f_{c,long}$ is the sum of an elastic strain $\varepsilon_{c,el}$ and a creep strain $\varepsilon_{c,c}$ in Equation 2-3:

$$\varepsilon_{c,long} = \varepsilon_{c,el} + \varepsilon_{c,c} = \varepsilon_{c,el} + \phi(t,\tau)\varepsilon_{c,el} = \frac{f_{c,long}}{E_c}\left[1+\phi(t,\tau)\right] \quad (2\text{-}3)$$

where

$\phi(t,\tau)$ = creep function

t = the age of the concrete

τ = the age when the stress $f_{c,long}$ is applied

Equation 2-4 expresses the creep function as (Menn 1986):

$$\phi(t,\tau) = \phi_n k(\bar{\tau})\, f\,(t-\tau) \quad (2\text{-}4)$$

where

ϕ_n = the creep coefficient that depends on material properties and environmental conditions

$k(\bar{\tau})$ = a correction factor for the age of concrete at time of loading

$f\,(t-\tau)$ = the time-varying behavior of creep and depends on an effective thickness parameter.

Table 2-1 shows the various factors that affect concrete creep and shrinkage in ACI 209.2R-08 *Guide for Modeling and Calculating Shrinkage and Creep in Hardened Concrete* (ACI 2008).

Table 2-1. Factors Affecting Concrete Creep and Shrinkage (ACI 2008)

Factors			Variables considered
Concrete (creep and shrinkage)	Concrete composition	Cement paste content	Type of cement
		Water-cement ratio	Slump
		Mixture proportions	Air content
		Aggregate characteristics	Fine aggregate percentage
		Degrees of compaction	Cement content
	Initial curing	Length of initial curing	Moist cured
			Steam cured
		Curing temperature	Moist cured
			Steam cured
		Curing humidity	Relative humidity
Member geometry and environment (creep and shrinkage)	Environment	Concrete temperature	Concrete temperature
		Concrete water content	Ambient relative humidity
	Geometry	Size and shape	Volume-surface ratio or minimum thickness
Loading (creep only)	Loading history	Concrete age at load application	Moist cured
			Steam cured
		During of loading period	Sustained load
		Duration of unloading period	—
		Number of load cycles	—
	Stress conditions	Type of stress and distribution across the section	Compressive stress
		Stress/strength ratio	Stress/strength ratio

Since the adoption of the current pre-stress loss provisions in the AASHTO LRFD, the accuracy and usability of the provisions have been called into question. For example, a study comparing measured and calculated pre-stress losses found a significant discrepancy in the time-dependent losses of high-strength concrete bulb-tee girders (Roller et al. 2011). Brewe observed that the AASHTO LRFD refined method underestimates the total pre-stress losses for all beams by an average of 22% (Brewe et al. 2008). Garber discussed that the current refined estimation method resulted in underestimation of the pre-stress loss by nearly half (Garber et al. 2013). Mertol et al. (2010) investigated creep and shrinkage of high-strength concrete of which

compressive strengths were 10 ksi, 14 ksi, and 18 ksi. The study showed that the creep coefficient in AASHTO LRFD (AASHTO 2017) was closer to the measured value for moist-cured, high-strength concrete specimens but overestimated the measured value for heat-cured specimens. For shrinkage strain, AASHTO LRFD provided reasonably good predictions compared to the measured strains except that the predicted shrinkage strains are higher than the measured values at an early age. In addition, there was less shrinkage for heat-cured specimens than for the moist-cured cylinders. The difference in the shrinkage having different strength (10 ksi to 18 ksi) was small.

Based on measured pre-stress loss data, Figure 2-7 compares different methods for estimating pre-stress losses (Garber et al. 2016). The Precast/Prestressed Concrete Institute (PCI) simplified method and 2004 AASHTO LRFD provisions are conservative in the estimation of the final pre-stress loss, whereas the other methods generate many cases where measured pre-stress losses are significantly larger than estimated losses. It was mentioned that the current provisions are less conservative and significantly more complex without accurately predicting pre-stress losses.

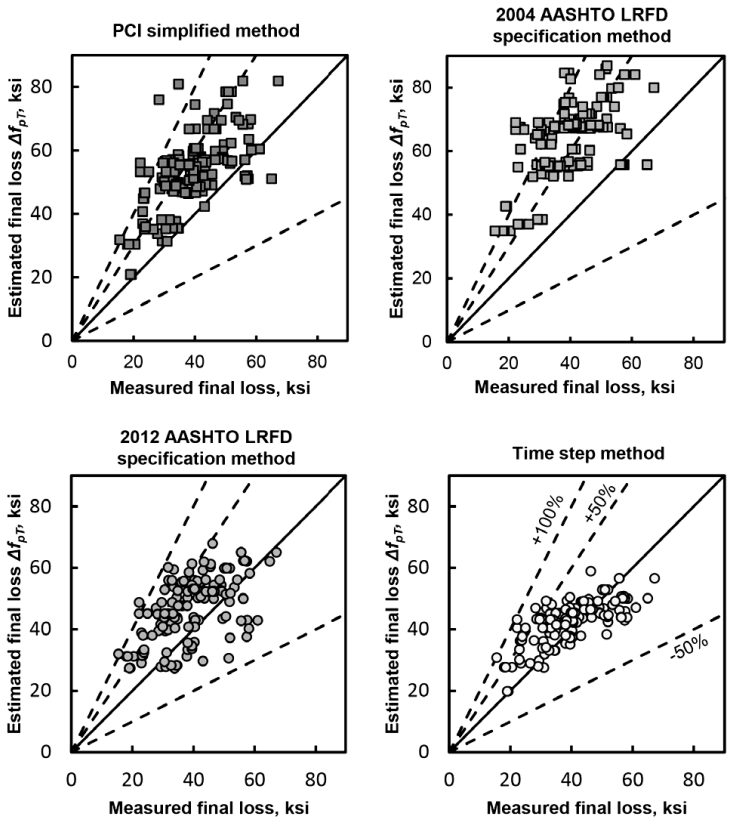

Figure 2-7. Estimated and Measured Pre-stress Losses (Garber et al. 2016)

2.2 Design Provisions in AASHTO LRFD (2017)

The pre-stress loss provisions in AASHTO LRFD were based on findings in NCHRP Project 18-07 (AASHTO 2017, Tadros et al. 2003). Equation 2-5 represents the total pre-stress loss as:

$$\Delta f_{pT} = \Delta f_{pES} + \Delta f_{pLT} \tag{2-5}$$

where

Δf_{pES} = instantaneous loss due to elastic shortening in members and

Δf_{pLT} = the sum of time-dependent losses.

For the estimation of the time-dependent losses, two methods were provided: approximate estimation and refined estimation. The approximate estimation method was developed for pre-stressed, I-beams and inverted tee beams with a compositely built concrete deck. The method assumes that moment from live load is about 1/3 of the total load moments. Therefore, the application of the approximate estimation method to DBT girders is questionable, and modification of the method may be necessary.

2.2.1 Instantaneous Pre-stress Losses

Interpretation of concrete strain prior to transfer, especially in high-strength concrete, is rather complicated. When pre-stressing force is released to the concrete and the temperature of the concrete is still elevated due to hydration and curing, the amount of pre-stressing force applied to the girder is significantly impacted by the temporary high temperature. Equation 2-6 represents strand stress loss due to a temperature rise, ΔT (Tadros et al. 2003):

$$\Delta f_{pt} = \alpha_s E_p \Delta T \tag{2-6}$$

where

Δf_{pt} = pre-stress changes (loss or gain) due to temperature change

α_s = the coefficient of the thermal expansion of steel

E_p = modulus of elasticity of pre-stressing strands

Equation 2-7 shows pre-stress loss due to the elastic shortening of pre-stressing strands [AASHTO 5.9.3.2.3a-1]:

$$\Delta f_{pES} = \frac{E_p}{E_{ct}} f_{cgp} \tag{2-7}$$

where

Δf_{pES} = pre-stress loss due to elastic shortening (ksi)

E_p = modulus of elasticity of pre-stressing steel (ksi)

E_{ct} = modulus of elasticity of concrete at transfer or time of load application (ksi)

f_{cgp} = concrete stress at the center of gravity of pre-stressing tendons due to the pre-stressing force immediately after transfer and the self-weight of the member at the section of maximum moment (ksi)

Historically, the conservative approach is to account for the effect of elastic deformation to occur at all stages of loading in the calculation of elastic shortening and creep losses considering only the pre-stress force present after transfer. Assume pre-stress to be 90% of the initial pre-stress before transfer and iterate the analysis until achieve acceptable accuracy. When using transformed section properties, treat the pre-stressing strand and the concrete together as a composite section. The effective stress in these strands consists of the sum of the Δf_{pES} values that must be included. However, analysis with gross (or net) section properties involves using the effective stress in the strands at any given stage of loading to determine the pre-stress force and resulting concrete stresses.

2.2.2 Time-Dependent Pre-stress Losses

In the refined estimation method, Equation 2-8 calculates the time-dependent pre-stress loss [AASHTO 5.9.3.4.1-1].

$$\Delta f_{pLT} = \left(\Delta f_{pSR} + \Delta f_{pCR} + \Delta f_{pR1}\right)_{id} + \left(\Delta f_{pSD} + \Delta f_{pCD} + \Delta f_{pR2} - \Delta f_{pSS}\right)_{df} \quad (2\text{-}8)$$

where

Δf_{pSR}= pre-stress loss due to shrinkage of girder concrete between transfer and deck placement

Δf_{pCR} = pre-stress loss due to creep of girder concrete between transfer and deck placement

Δf_{pR1}= pre-stress loss due to relaxation of pre-stressing strands between time of transfer and deck placement

Δf_{pR1}= pre-stress loss due to relaxation of pre-stressing strands in composite section between time of deck placement and final time

Δf_{pSD}= pre-stress loss due to shrinkage of girder concrete between time of deck placement and final time

Δf_{pCD} = pre-stress loss due to creep of girder concrete between time of deck placement and final time

Δf_{pSS}= pre-stress gain due to shrinkage of deck in composite section

$\left(\Delta f_{pSR} + \Delta f_{pCR} + \Delta f_{pR1}\right)_{id}$= sum of time-dependent pre-stress losses between transfer and deck placement

$\left(\Delta f_{pSD} + \Delta f_{pCD} + \Delta f_{pR2} - \Delta f_{pSS}\right)_{df}$= sum of time-dependent pre-stress losses after deck placement

For the estimation of each component in time-dependent pre-stress losses, the concrete strain is estimated based on the stress-strain relationship of slow-loading which can be represented by elastic modulus, $E_c^{"}$, in Equation 2-9: (Tadros et al. 2003):

$$E_c^{"} = \frac{E_{ci}}{1 + \chi \psi_b \left(t_f, t_i\right)} \tag{2-9}$$

where

E_{ci} = the concrete elastic modulus at pre-stress transfer,

$\chi = 0.7$ = the relaxation coefficient, and

$\psi_b \left(t_f, t_i\right)$ = the creep coefficient.

The creep coefficient in Equation 2-10 is the ratio of creep strain at time $t = t_f$ to elastic strain when applying a load at time $t = t_i$ and holding it constant (Tadros et al. 2003).

$$\psi_b(t_f, t_i) = \frac{\varepsilon_{cc}}{\varepsilon_e} = \psi_u \cdot \gamma_{cr} = 1.9 \cdot \left(k_{td} k_s k_{hc} k_f t_i^{-0.118}\right) \tag{2-10}$$

where

ψ_u = an ultimate creep coefficient

k_{td} = the time-development factor

k_s = the factor for the effect of the volume-to-surface ratio

k_{hc} = the humidity factor

k_f = the factor for effect of concrete strength

Correction factors are used in various prediction methods to modify the ultimate values of creep coefficient and shrinkage strain of concrete for any period. Factors are introduced to account as much as possible for the average conditions commonly encountered in practices; such as 70% annual average ambient relative humidity, V/S ratio of 3.5in., loading age of 1 day for precast pre-tensioned members and 7 days for cast-in-place deck slabs, and accelerated curing for 1 day or moist curing for 7 days. (Tadros et al. 2003)

For the ambient relative humidity, equations can apply the range of 30% to 80% encountered in the United States to the humidity factors for shrinkage and creep, as used in Equation 2-11 and Equation 2-12 (Tadros et al. 2003):

$$\text{Shrinkage: } k_{hs} = 2.00 - 0.0143H \tag{2-11}$$

$$\text{Creep: } k_{hc} = 1.56 - 0.008H \tag{2-12}$$

where H = relative humidity (%).

The pre-stress loss due to shrinkage of girder concrete between the time of transfer and the time of deck placement shall be determined in Equation 2-13 and Equation 2-14 [AASHTO Equations 5.9.5.4.2a-1 and 5.9.5.4.2a-2] as:

$$\Delta f_{pSR} = \varepsilon_{bid} E_p K_{id} \tag{2-13}$$

$$K_{id} = \frac{1}{1 + \frac{E_p}{E_{ci}} \frac{A_{ps}}{A_g} \left(1 + \frac{A_g e_{pg}^2}{I_g}\right)[1 + 0.7\psi_b(t_f, t_i)]} \tag{2-14}$$

where

ε_{bid} = concrete shrinkage strain of girder between the time of transfer and deck placement per AASHTO Equation 5.4.2.3.3-1 (in. / in.)

K_{id} = transformed section coefficient that accounts for time-dependent interaction between concrete and bonded steel in the section being considered for time period between transfer and deck placement

e_{pg} = eccentricity of pre-stressing force with respect to the centroid of girder (in.); positive in common construction where it is below girder centroid

$\psi_b(t_f, t_i)$ = girder creep coefficient at final time due to loading introduced at transfer per AASHTO Equation 5.4.2.3.2-1

t_f = final age (day)

t_i = age of concrete at time of transfer (day)

The pre-stress loss due to shrinkage of girder concrete between the time of deck placement and the final time found in Equation 2-15 and Equation 2-16 [AASHTO Equation 5.9.3.4.3a-1 and 5.5.9.4.3a-2] shall be determined as:

$$\Delta f_{pSD} = \varepsilon_{bdf} E_p K_{df} \tag{2-15}$$

$$K_{df} = \frac{1}{1 + \frac{E_p}{E_{ci}} \frac{A_{ps}}{A_c} (1 + \frac{A_c e_{pc}^2}{I_c})[1 + 0.7\psi_b(t_f, t_i)]} \tag{2-16}$$

where

ε_{bdf} = shrinkage strain of girder between time of deck placement and final per AASHTO Equation 5.4.2.3.3-1

K_{df} = transformed section coefficient that accounts for time-dependent interaction between concrete and bonded steel in the section being considered for time period between deck placement and final time

e_{pc} = eccentricity of pre-stressing force with respect to centroid of composite section (in.)

positive in typical construction where pre-stressing force is below centroid of section

A_c = area of section calculated using the gross composite concrete section properties of the girder and the deck and the deck-to-girder modular ration (in.^{2})

I_c = moment of inertia of section calculated using the gross composite concrete section properties of the girder and the deck and the deck-to-girder modular ration (in.^{4})

The pre-stress loss due to creep of girder concrete between the time of transfer and the time of deck placement in Equation 2-17 [AASHTO Equation 5.9.3.4.2b-1] shall be determined as:

$$\Delta f_{pCR} = \frac{E_p}{E_{ci}} f_{cgp} \psi_b(t_d, t_i) K_{id} \qquad (2\text{-}17)$$

where

Δf_{pCR} = pre-stress loss due to creep of concrete between time of transfer and deck placement

$\psi_b(t_d, t_i)$= girder creep coefficient at time of deck placement due to loading per AASHTO Equation 5.4.2.3.2-1

t_d = age at deck placement (day)

The pre-stress loss due to creep of girder concrete between time of deck placement and final time in Equation 2-18 [AASHTO Equation 5.9.5.4.3b-1] shall be determined as:

$$\Delta f_{pCD} = \frac{E_p}{E_{ci}} f_{cgp} \left[\psi_b(t_f, t_i) - \psi_b(t_d, t_i) \right] K_{df} + \frac{E_p}{E_c} \Delta f_{cd} \psi_b(t_f, t_d) K_{df} \qquad (2\text{-}18)$$

where

Δf_{pCD} = the change in pre-stress (loss is positive, gain is negative) due to creep of girder concrete between time of deck placement and final time

Δf_{cd} = change in concrete stress at centroid of pre-stressing strands due to long-term losses between transfer and deck placement, combined with deck weight and superimposed loads (ksi)

$\psi_b(t_f, t_d)$ = girder creep coefficient at final time due to loading at deck placement per AASHTO Equation 5.4.2.3.2-1

The pre-stress loss due to relaxation of pre-stressing strands between the time of transfer and the time of deck placement shall be determined in Equation 2-19 [AASHTO Equation 5.9.3.4.2c-1] as:

$$\Delta f_{pR1} = \frac{f_{pt}}{K_L}\left(\frac{f_{pt}}{f_{py}} - 0.55\right) \qquad (2\text{-}19)$$

where

Δf_{pR1} = The pre-stress loss due to relaxation of pre-stressing strands between time of transfer and deck placement, may be assumed equal to 1.2ksi for low-relaxation strands.

K_L = factor accounting for type of steel taken as 30 for low relaxation strands and 7 for other pre-stressing steel, unless more accurate manufacturer's data are available

f_{pt} = stress in pre-stressing strands immediately after transfer, taken not less than 0.55 f_{py} in AASHTO Equation 5.9.3.4.2c-1

Equation 2-20 gives a more accurate prediction of relaxation loss between transfer and deck placement (Tadros et al. 2003):

$$\Delta f_{pR1} = \left[\frac{f_{pt}}{K_L'}\frac{log(t)}{log(t_i)}\left(\frac{f_{pt}}{f_{py}} - 0.55\right)\right]\left[1 - \frac{3(\Delta f_{pSR}+\Delta f_{pCR})}{f_{pt}}\right]K_{id} \qquad (2\text{-}20)$$

where

K_L' = factor accounting for type of steel, equal to 45 for low relaxation steel

K_{id} = factor accounting for restraint of concrete member caused by bonded reinforcement = 0.8

t = time between strand tensioning and deck placement (day) = 120 days

t_i = 0.75 day

$$\left[1-\frac{3\left(\Delta f_{pSR}+\Delta f_{pCR}\right)}{f_{pt}}\right] = 0.67$$

The pre-stress loss due to relaxation of pre-stressing strands in composite section between time of deck placement and final time, Δf_{pR2}, shall be determined in Equation 2-21 [AASHTO Equation 5.9.3.4.3c-1] as:

$$\Delta f_{pR2} = \Delta f_{pR1} \qquad (2\text{-}21)$$

The pre-stress gain due to shrinkage of deck composite section, Δf_{pSS}, shall be determined in Equation 2-22 and in Equation 2-23 [AASHTO Equation 5.9.3.4.3d-1 & 5.9.3.4.3d-2] as:

$$\Delta f_{pSS} = \frac{E_p}{E_c} f_{cdf} K_{df}\left[1+0.7\psi_b(t_f,t_d)\right] \qquad (2\text{-}22)$$

$$\Delta f_{cdf} = \frac{\varepsilon_{ddf} A_d E_{cd}}{[1+0.7\Psi_d(t_f,t_d)]}\left[\frac{1}{A_g} - \frac{e_{pc}e_d}{I_c}\right] \qquad (2\text{-}23)$$

where

Δf_{cdf} = change in concrete stress at centroid of pre-stressing strands due to shrinkage of deck concrete (ksi)

ε_{ddf} = shrinkage strain of deck concrete between placement and final time per AASHTO Equation 5.4.2.3.3-1 (in./in.)

A_d = area of deck concrete (in.^{2})

E_{cd} = modulus of elasticity of deck concrete (ksi)

e_d = eccentricity of deck with respect to the gross composite section, positive in typical construction where deck is above girder (in.)

$\Psi_d(t_f, t_d)$ = creep coefficient of deck concrete at final time due to loading introduced shortly after deck placement

2.3 Other Design Provisions

For pre-stress loss estimation, three methods have been used: lump-sum estimates, rational approximate methods, and detailed time-dependent analyses. The approximate estimation method of time-dependent losses (section 5.9.3.3) in AASHTO LRFD and the total-loss method in the PCI Design Handbook are lump-sum estimate methods (AASHTO 2017, PCI 2010). The refined estimation of time-dependent losses method (section 5.9.3.4) in AASHTO LRFD and a method in the PCI Design Handbook classify as rational approximate methods. Detailed time-dependent analyses may provide accurate prediction of pre-stress losses. Some of

these methods are presented in the PCI Bridge Design Manual (PCI 2000). In the present study, the following methods are of primary concern.

- 2004 AASHTO Lump-sum method
- 2004 AASHTO Refined method
- 2017 AASHTO Approximate estimation
- 2017 AASHTO Refined estimation

In NCHRP report 496, the final form of the approximate method of pre-stress loss formula is shown as (Tadros et al. 2003) in Equations 2-24 through 2-26:

$$\Delta f_{pLT} = 10.0 \frac{f_{pi} A_{ps}}{A_g} \gamma_h \gamma_{st} + 12.0 \gamma_h \gamma_{st} + 2.5 \tag{2-24}$$

$$\gamma_h = 1.7 - 0.01H \tag{2-25}$$

$$\gamma_{st} = \frac{5}{1 + f_{ci}^{'}} \tag{2-26}$$

where

γ_h = correction factor for relative humidity of the ambient air

γ_{st} = correction factor for specified concrete strength at time of pre-stress transfer to concrete member

A_{ps} = area of pre-stressing steel (in^2)

f_{pi} = pre-stressing steel stress immediately prior to transfer (ksi)

The following assumptions were made to arrive at the approximate method coefficients:

(a) Calculate pre-stress losses for conditions at the maximum positive moment section.

(b) No mild steel reinforcement exists at that section

(c) Elastic losses at transfer or elastic gains due to application of external loads are not considered.

(d) Pre-stress is transferred to the concrete at 1 day in accelerated plant curing conditions.

(e) The cast-in-place deck weight (composite construction) is applied to the precast concrete section without any shoring after at least 28 days from the time of pre-stress transfer.

(f) V/S ratio for the girder cross section is 3 in. to 4 in.

In the third edition of the AASHTO LRFD specifications, pre-stress losses due to concrete creep and shrinkage were determined from Equation 2-27 and Equation 2-28 (AASHTO 2004):

$$\Delta f_{pCR} = 12.0 f_{cgp} - 7.0 \Delta f_{cdp} \quad (2\text{-}27)$$

$$\Delta f_{pSR} = 17.0 - 0.15H \quad (2\text{-}28)$$

where

f_{cgp} = the concrete stress at the center of gravity of the pre-stressing

Δf_{cdp} = the concrete stress change due to permanent loads

H = average relative humidity (%).

The *Alaska Bridges and Structures Manual* (ADOT&PF 2017) was mainly based on the 6th edition of the AASHTO LRFD (2012), but provisions for the estimation of time-dependent pre-stress losses for DBT girders in Equation 2-29 were adopted from the lump-sum method in the 3rd edition (or before) of the AASHTO LRFD. Specifically, the equation of average loss for

single T or double T girders was adopted with a pre-stress loss reduction of -8 ksi for low-relaxation strands. In this equation, the sum of time-dependent pre-stress losses is expressed as a function of concrete strength, $f_c^{'}$.

$$\Delta f_{pLT} = 33\left[1 - 0.15\left(\frac{f_c^{'} - 6}{6}\right)\right] - 2 \quad (ksi) \tag{2-29}$$

The 28 day compressive strength of concrete in structural elements can be found in the ADOT&PF tables in Chapter 14 regarding structural concrete (ADOT&PF 2017). Normal weight concrete varies between 145 pcf for cast-in-place concrete, and 155 pcf for precast concrete excluding the weight of the internal steel reinforcement. The common sizes for the pre-stressing strands used in bridge construction are 0.5 inches in diameter and 0.6 inches in diameter. For girders within Alaska, the diameter of the pre-stressing strands in pre-tensioned girders is 0.5 inches, while the diameter is typically 0.6 inches for girders fabricated outside Alaska.

CHAPTER. 3 CONCRETE CREEP TEST SETUP

The amount of concrete creep that a particular concrete experiences is difficult to estimate accurately unless concrete cylinder tests are conducted to determine the creep characteristics. Without such tests, accuracies of better than ±30% should not be expected (Collins and Mitchell 1997). From the measurement of small size test specimens, it was observed that most of the pre-stress loss occurred in the first 168 days, and the loss increases significantly within the first 6 months (Brewe et al. 2008).

In the present research, the project fabricated two concrete creep test frames based on ASTM C 512 “Standard Test Method for Creep of Concrete in Compression” (ASTM 2015). The project placed one test frame in the structural engineering laboratory at University of Alaska Fairbanks (UAF) and located the other frame outside a building on the UAF campus under ambient environment conditions. The effects on concrete creep from the cold climate were evaluated by comparing the measured strain changes from the two test frames for 11 months (7/26/2017 – 6/21/2018).

3.1 Concrete Creep Test Frame

The project designed concrete creep test frames based on ASTM C 512 (ASTM 2015). The design for the apparatus is shown in Figure 3-1 with a maximum capacity of 192,000 lbf., and a maximum stress to the frame of 6,795 psi. In each of the test frames, two 6″×12″ cylindrical specimens were placed on top of one another with 1″ thick circular steel plates as spacers and tested under the same compression while an additional two specimens were placed unloaded near the frame.

The load was applied by means of a hydraulic jack, with a maximum capacity of 120,000 lbf., and monitored by a calibrated load cell. After reaching the desired load, the nuts on the threaded rods are turned so that they are snugly pressing against the plate underneath the hydraulic jack, holding the plate in position. After the nuts are securely positioned, the jack can be removed from the test frame and used to set the load on another test frame. After the jack is removed, the 9 sets of springs (D2 inner and D2 outer types) in the frame maintain the load applied to the specimens consistently. The apparatus used standard railroad springs, which are much less expensive than custom-made springs, at the base of the frame as to apply equal force upward.

Each spring set consists of two springs. The spring constant of the outer spring, k_l, is 9,778 lbf/in, while the spring constant of the inner spring, k_s, is 3,520 lbf/in. When used as a set, the combined stiffness is 13,298 lbf/in, and the solid capacity is 21,345 lbf [4]. Under the maximum load, the set of springs deforms 1.61 inches. If all nine sets of springs are used, the maximum load, $C_{\max}$, that the springs can hold can be calculated to 192,000 lbf. The maximum stress, σ_{MAX}, that can be applied to a 6"×12"cylindrical concrete specimen in the creep frame can be calculated as 6,795 psi. In consideration that the concrete test specimens may be loaded up to 50% of its compressive strength in the creep test, this creep apparatus can be used to test concretes with a maximum ultimate compressive strength of 13,590 psi.

[4] Personal e-mail communication with a vendor.

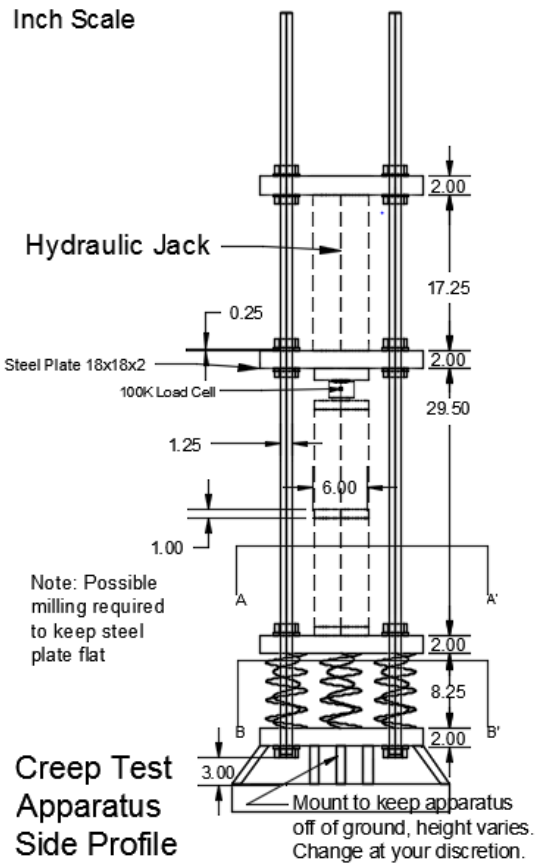

Figure 3-1. Creep Test Apparatus

When the concrete specimens are loaded in the creep frame, each of the four steel rods will carry one quarter of total load. The steel rods are 1.125 in. in diameter and are made of a high-strength alloy steel with a yield strength of 105 ksi. If the concrete specimens were loaded up to the maximum capacity of the creep apparatus, 192,000 lbf, the maximum stress in the steel rods would be equal to 48,300 psi. This maximum possible stress in the steel rod is less than half of the yield strength of the steel, 105,000 psi.

As the concrete specimens are loaded in the creep frame, the rectangular steel plates, which are in between each cylinder, deflect slightly. To keep the loading surfaces flat and the test specimens vertical when the load is applied, place three 1-inch thick circular steel plates with a diameter of 6 inches on the top and bottom of the stack of concrete test specimens and in between the cylinders.

As the concrete specimens creep under the sustained load in the creep frame, the load applied on the concrete reduces. Calculate the load relaxation due to the creep deformation of the concrete specimens by multiplying the total creep deformation by the total spring constant of the springs, as follows:

Load Relaxation = (Total Spring Constant) × (Creep Deformation)
= (Total Spring Constant) × (Creep Strain) × number of specimens × 12 in.

When all nine sets of springs are used, the total spring constant is equal to 119,682 lbf/in. Table 3-1 presents the load relaxation of the creep frame for various values of creep strains for the case when all nine sets of springs are used. It compares two test setup cases, two specimens and three specimens. Depending on the creep strain and the number of specimens, re-adjustment of load may be necessary to maintain constant load on the concrete specimens.

Table 3-1. Load Relaxation in the Creep Apparatus due to Creep Strain of Concrete

Creep Strain	5.0×10^{-5}	1.0×10^{-4}	5.0×10^{-4}	1.0×10^{-3}	2.0×10^{-3}
Load Relaxation (lbf) : 2 specimens	140	280	1400	2800	5600
Load Relaxation (lbf) : 3 specimens	210	420	2100	4200	8400

3.2 Concrete Cylinder Specimens

The project used a single batch of concrete to mold specimens for compression and stress-strain tests at AggPro in Anchorage, Alaska, during a girder pour for the 76th Avenue Undercrossing Bridge on July 12, 2017. The design concrete strength was $f_{ci}^{'} = 7000\,psi$ at stress transfer and $f_{c}^{'} = 8500\,psi$ at 28 days, as found in the submitted and approved girder plan in Appendix A.

ADOT&PF approved the concrete mix design submitted by the project. The mix ingredients follow:

- Cement

  ABI Type III Cement was used in the batches.

- Coarse Aggregate

  The coarse aggregate used was AASHTO Gr. # 67 with a saturated surface dry (SSD) Specific Gravity of 2.70, Absorption Percent of 0.69, and a Dry-Rodded Unit Weight of 110.7.

- Intermediate Aggregate

  The intermediate aggregate used was AASHTO Gr. # 8 with an SSD Specific Gravity of 2.69, an Absorption Percent of 0.62, and a Dry-Rodded Unit Weight of 110.3.

- Fine Aggregate

  The fine aggregate used was AASHTO Gr. # M6 with a SSD Specific Gravity of 2.64, Absorption percent of 1.39, and a Fineness Modulus of 2.76.

- Water-Reducing Admixture

The water-reducing admixture used included BASF PS 1466: a ready-to-use high-range water-reducing admixture effective in assisting with workability.

Figures 3-2 through 3-4 illustrate the grain size distribution charts for the materials pit that produced the aggregates for the concrete mix design.

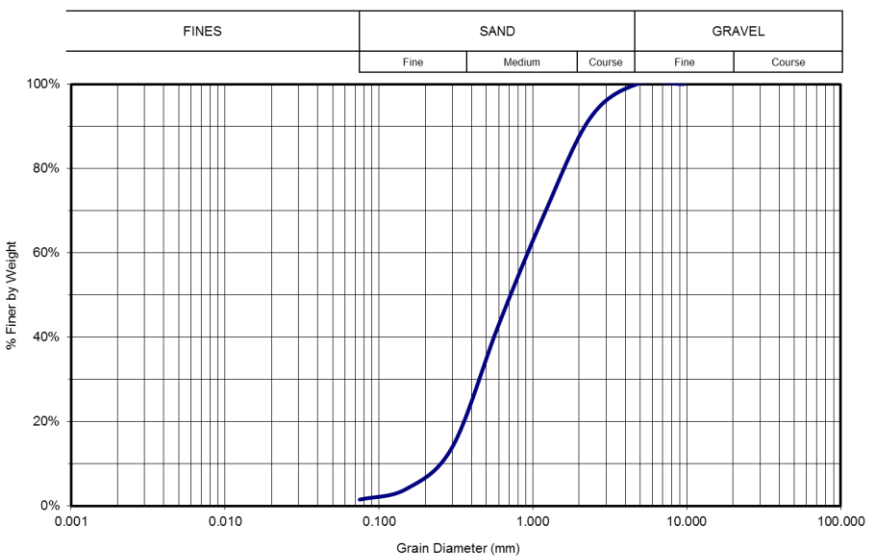

Figure 3-2. Fine Concrete Aggregate Grain Size Distribution

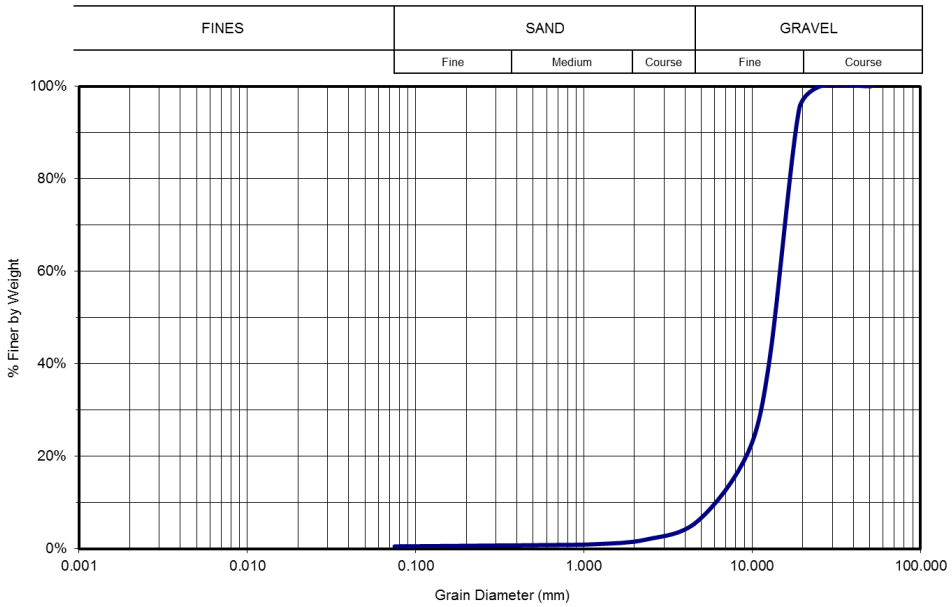

Figure 3-3. Coarse Concrete Aggregate Grain Size Distribution

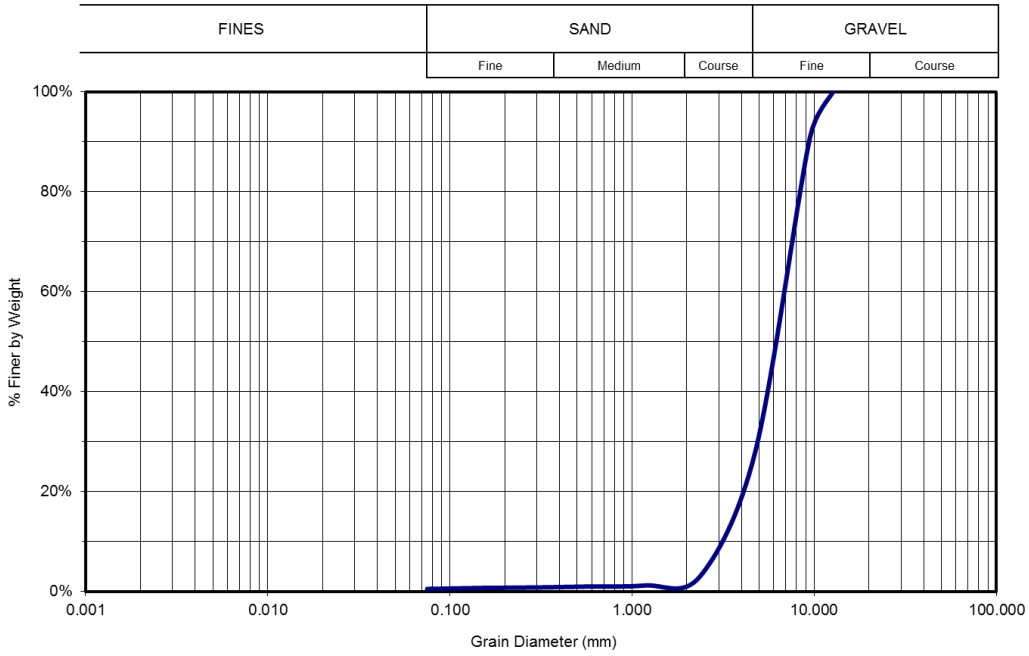

Figure 3-4. 3/8” Aggregate Grain Size Distribution

The concrete specimens were made in conformance with ASTM standard C31 “Making and Curing Concrete Test Specimens in the Field” utilizing a tamping rod as seen in Figure 3-5 (ASTM 2012). During the girder pour, 24 cylinders of size 4″×8″ and 15 cylinders of size 6″×12″ were made and cured on site. The project place thermistors inside the cylinders. Figure 3-6 shows the completion of the fieldwork with the sensors in position. The superintendent of operations from AggPro also made 3 cylinders, following the metal mold and vibratory method, to be steam cured along with the girder. Testing the following morning checked the cylinders for compression strength to ensure the strength at force transfer. A technician from DOWL HKM, who specializes in quality assurance for concrete, also measured slump (9 inches), percent air entrained (2.5%), unit weight (152.2 pcf), ambient temperature (57°F), and concrete temperature (64°F) [5].

Transportation of the concrete cylinders from AggPro in Anchorage to Fairbanks followed ASTM C31 section 11 “Transportation of Specimens to Laboratory”. The cylinders were capped and placed at the bottom of a 5-gallon bucket to remain flat; sand was poured around them to maintain a solid, vertical surrounding. The transportation time shall not exceed 4 hours according to the specification, however, ADOT&PF in Alaska realizes that this feat is an impossibility in such a large state for certain locations. After leaving Anchorage around 10:00 am and arriving in Fairbanks roughly 6 hours later, the cylinders were stripped of their molds and placed in a lime bath at the ADOT&PF Northern Region Materials Lab.

[5] From a data sheet from DOWL HKM. Attached in Appendix B.

Figure 3-5. Making Concrete Test Specimens in the Field

Figure 3-6. Completion of Making Concrete Cylinders in the Field

3.3 Sensors and Data Acquisition System

The project placed two pairs of gage points with a gage distance of 8 inches in each concrete test specimen. A Demountable Mechanical Strain Gauge (DEMEC) was used to measure the change in distance between the gage points.

Once the cylinders reached the design strength at force transfer, they were prepared for the creep test. Placement of the cylinders into the loading frame required preparation of the gauge points and leveling the top and bottom with a diamond tipped saw. Holes drilled into the specimens at roughly 1 inch from the top and bottom, and approximately 8 inches apart from each other allowed the DEMEC strain gauge to measure the distance change. After the holes were drilled out to proper depth, an air compressor cleaned out the dust while gauge plugs with JBWeld epoxy were used to maintain a constant position within the cylinders, which can be seen in Figure 3-7. The thermistors were located at the center of the cylinder, as seen in Figure 3-8, with the ends protected and secured in place. Gauge points with a half-spherical shape are then screwed inside the plugs to allow an accurate center-to-center measurement.

Thermistors and load cells were connected to the Campbell Scientific CR1000 data logger located inside a weatherproof case. The load cells were calibrated before use to ensure accuracy.

Figure 3-7. Specimens Epoxied with Gauge Plugs

Figure 3-8. Specimens Pre-Loading Set Up with Thermistors

3.4 Ambient Temperature and Relative Humidity Data

As cylinder deformation was measured, indoor and outdoor temperature and relative humidity were recorded. The project obtained robust weather data from the closest in-service weather station, on West Ridge of the UAF campus. The station, FAOA2 College Observatory, is located at the Elvey building, providing an adequate comparison for obtaining records.

CHAPTER. 4 EXPERIMENTAL PROGRAMS

In the two creep test frames, two concrete cylinders stacked together were loaded with a target compression of 80,000 pounds on the 13th day after molding (7/25/2017). The target compression is roughly 33% of the compressive strength of the specimens on the 14th day following ASTM C512 (ASTM 2015). Once the target compression was reached, bolts were tightened, steel plates of the frame were fixed in position, and the hydraulic jack was demounted. Circular steel and rubber plates placed in between the cylinders equally distributed the load. Figures 4-1 and 4-2 show the two concrete creep frames under loading with the jack still in position.

Figure 4-1. Specimens Loading Set Up Indoor Frame

Figure 4-2. Specimens Loading Set Up Outdoor Frame

4.1 Compressive Strength of Concrete

The project tested compressive strength of the concrete at 3, 7, 14, 28, 56, 90, 189, and 365 days. 4″×8″ cylinders were stored in a lime bath at the ADOT&PF Regional lab in Fairbanks. Three cylinders were broken to failure in each test age following the ASTM standard C39 (ASTM 2018). Figure 4-3 shows an example of the loading apparatus for the 3-day test.

Figures 4-4 through 4-10 show the results of the strength tests for 3, 7, 14, and 28-day tests of the 4″×8″ cylinders. The cylinders can be seen breaking in the middle in earlier breaks, however, as the concrete gets harder, it starts to shear off at the corner.

Figure 4-3. 3-Day Break Cylinder Strength Test Loading

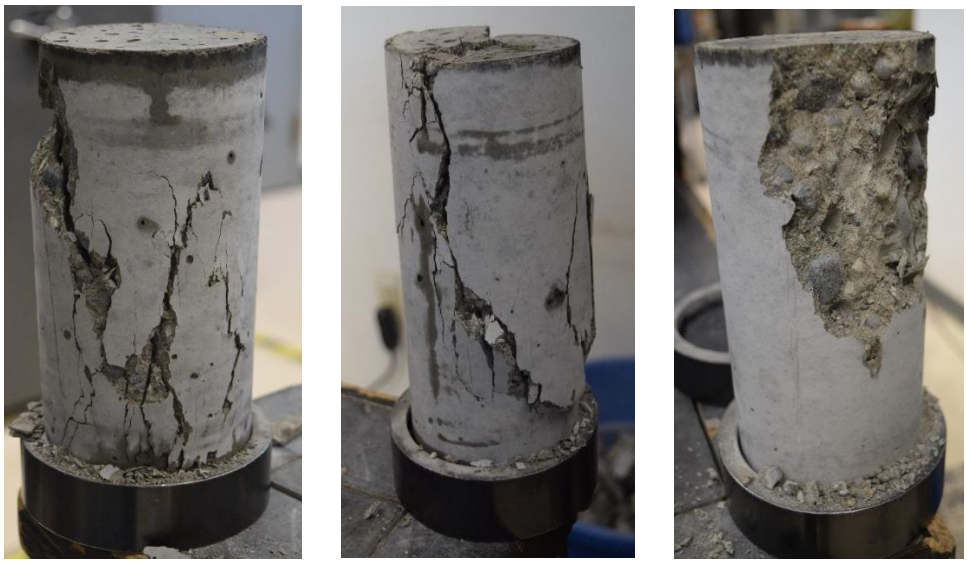

Figure 4-4. 3-Day Break Strength Test Results 1 through 3

Figure 4-5. 7-Day Break Cylinder Strength Test Loading

Figure 4-6. 7- Day Break Strength Test Results 1 through 3

Figure 4-7. 14-Day Break Strength Test Results 1 through 3

Figure 4-8. 28-Day Break Cylinder Strength Test Loading

Figure 4-9. 28- Day Break Strength Test Results 1 through 3 in Frame

Figure 4-10. 28-Day Breaks 1 Through 3

Table 4-1 shows the measured concrete strength. Figure 4-11 illustrates the relationship between the average compressive strength and age with a trend line, behaving as expected, increasing up to a maximum after a longer period of curing. As time increases, the average

compression strength increases up to the 56 day break. At 90 days the strength of the concrete decreases, however, the 189 and 365 day breaks showed the strength increased to its local maximum. The specified 28-day strength was 8,000 psi, and a probable 28-day strength was 10,000 psi in the concrete mix design report. From the strength test result, the 28-day strength was 9,119 psi which was less than the probable strength but greater than the specified strength.

Table 4-1. Compressive Strength Test Results

Age (Days)	Test #1 (psi)	Test #2 (psi)	Test #3 (psi)	Average (psi)
3	6,909	6,750	6,788	6,816
7	7,935	8,156	7,957	8,016
14	8,761	8,654	8,545	8,654
28	9,609	9,206	8,543	9,119
56	10,317	9,597	10,569	10,161
90	9,845	9,927	9,467	9,746
189	11,993	11,175	11,625	11,598
365	11,719	12,146	11,873	11,913

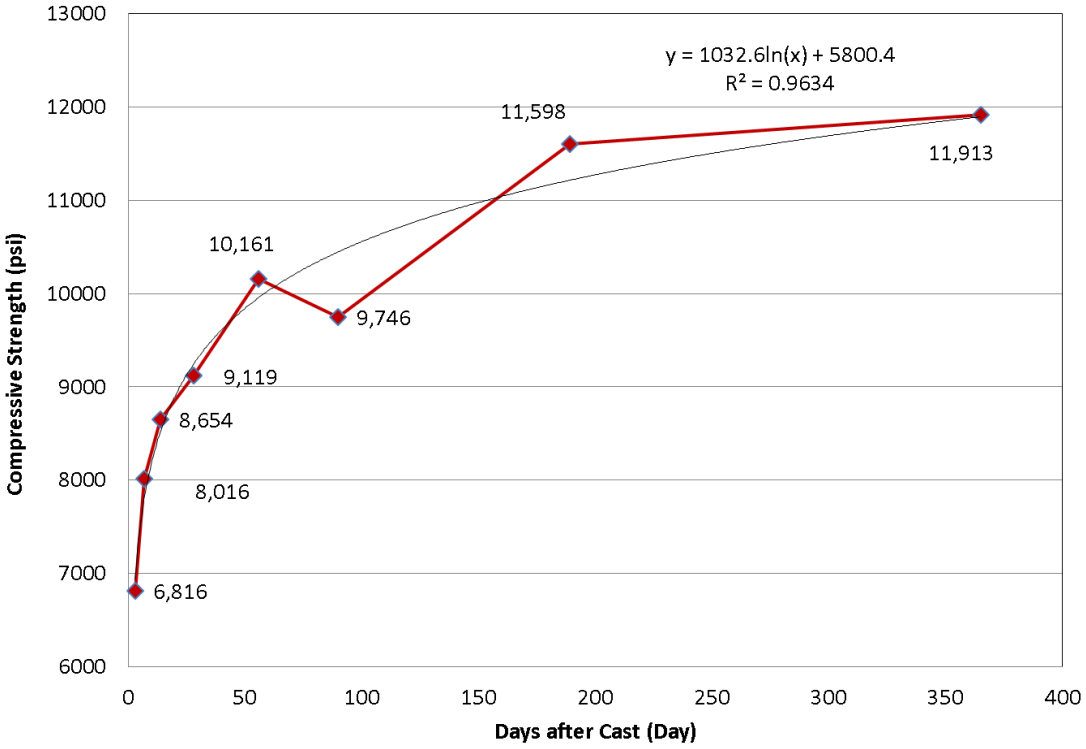

Figure 4-11. Compressive Strength (psi) vs. Time (Days)

4.2 Elastic Modulus of Concrete

The stress-strain tests of the cylinders carried out on a Forney compression machine in the Structural Materials Lab at UAF, as shown in Figure 4-12 following the ASTM C469 "Standard Test Method for Static Modulus of Elasticity and Poisson's Ratio of Concrete" (ASTM 2014). The project used a compressometer to measure the stress-strain of the cylinder as it is loaded utilizing a digital readout. The first loading trial is not recorded, per ASTM C469, and the following two readings are then measured and recorded. The following Figures 4-13 through 4-16 show the stress-strain in graphical format for the 14, 29, 189, and 365 days tests.

Figure 4-12. Stress-Strain Test using Forney Compression Machine & Compressometer

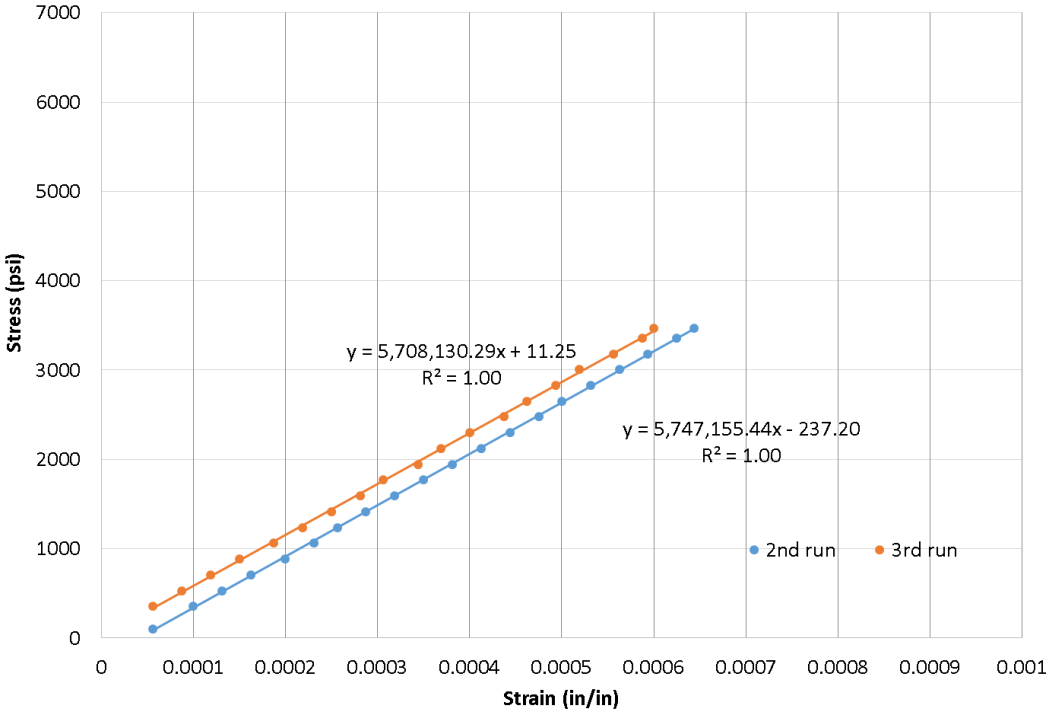

Figure 4-13. 14-day stress-strain test

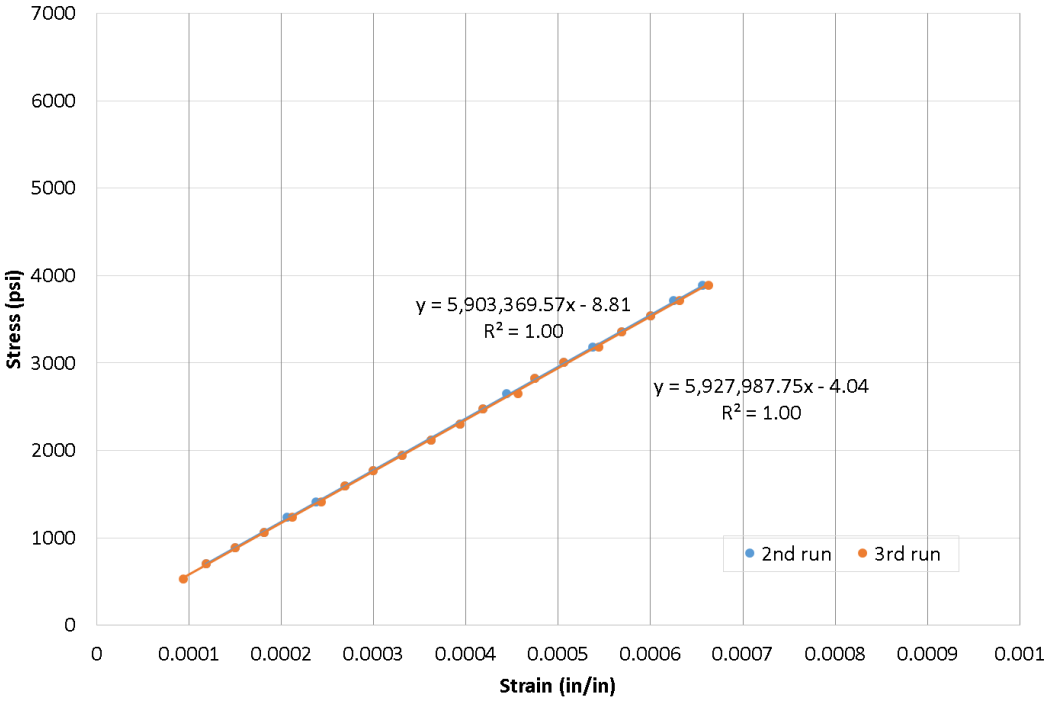

Figure 4-14. 29-day stress-strain test

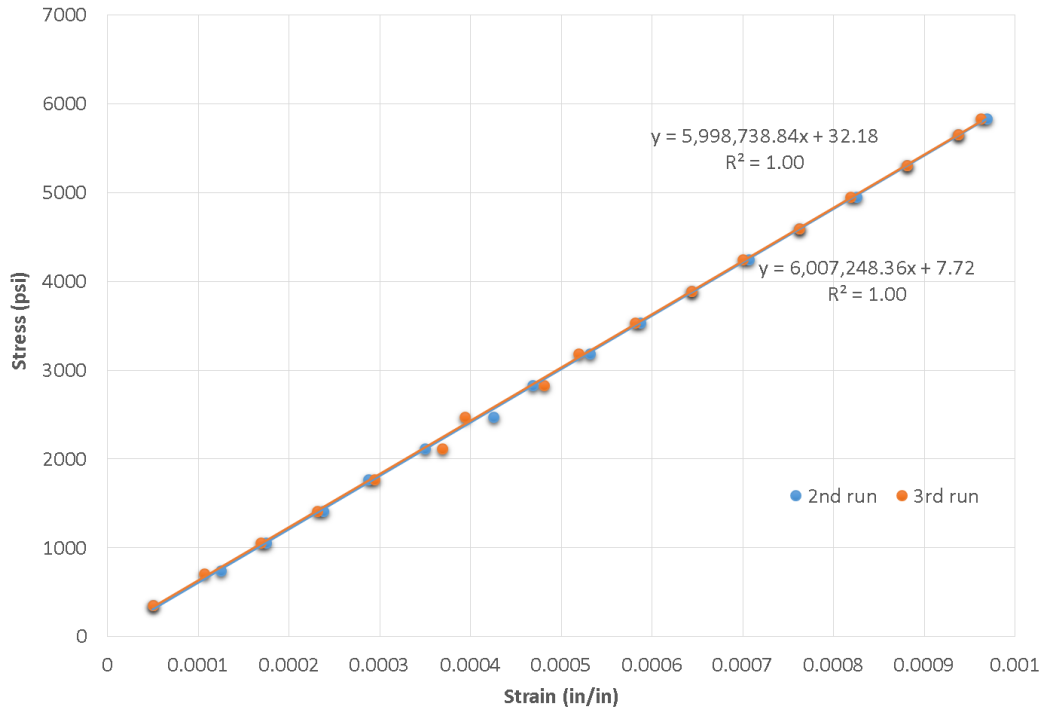

Figure 4-15. 189-day stress-strain test

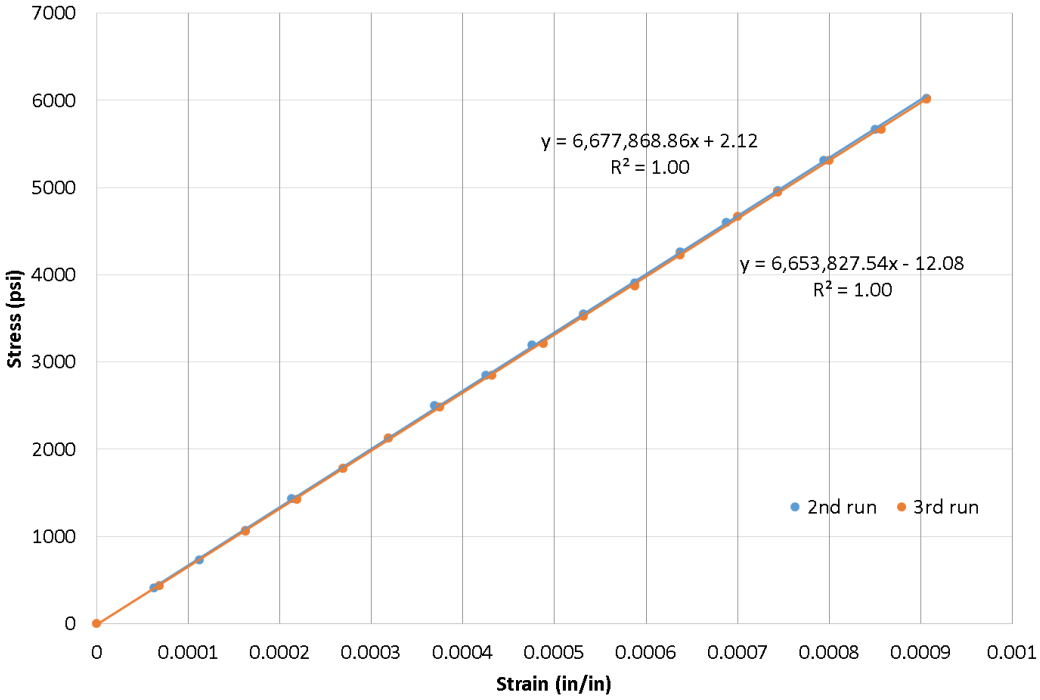

Figure 4-16. 365-day stress-strain test

Table 4-2 summarizes measured elastic modulus values and compares them with calculated values based on measured concrete compressive strength. The values in "AASHTO (8^{th})" were calculated from Equation 4-1 while the values in "AASHTO (7^{th})" were calculated from a traditional equation in Equation 4-2 (AASHTO 2014, 2017).

$$E_c = 120,000 K_1 w_c^{2.0} f_c'^{0.33} \quad (4\text{-}1)$$

$$E_c = 33,000 K_1 w_c^{1.5} \sqrt{f_c'} \quad (4\text{-}2)$$

where

K_1 = correction factor for source of aggregate (1.0 unless determined by physical test)

w_c = the unit weight of concrete (kcf)

f_c' = the compressive strength of concrete (ksi)

The unit weight of concrete used in the calculation was $w_c = 151.5 pcf$ from the concrete design mix document. The average concrete strength measured from 4″×8″ specimens in Table 4-1 was also used in the calculation.

Table 4-2. Comparison of Concrete Elastic Modulus (psi)

Day	2nd run	3rd run	Average	AASHTO (8th)	AASHTO (7th)
3				5,188,768	5,069,952
7				5,474,098	5,489,181
14	5,747,155	5,708,130	5,727,643	5,614,096	5,688,318
28	5,927,988	5,903,370	5,915,679	5,712,081	5,687,718
56				5,919,643	6,326,301
90				5,838,807	5,987,411
189	6,007,248	5,998,739	6,002,994	6,183,729	6,634,937
365	6,677,869	6,653,828	6,665,848	6,238,637	6,705,112

Figure 4-17 compares the measured and calculated elastic moduli. At 28 days, the calculated values are comparable with the measured one, but they become different as it approaches 365 days. The calculated value based on AASHTO 7th ed. is closer to the measured value at 365 days.

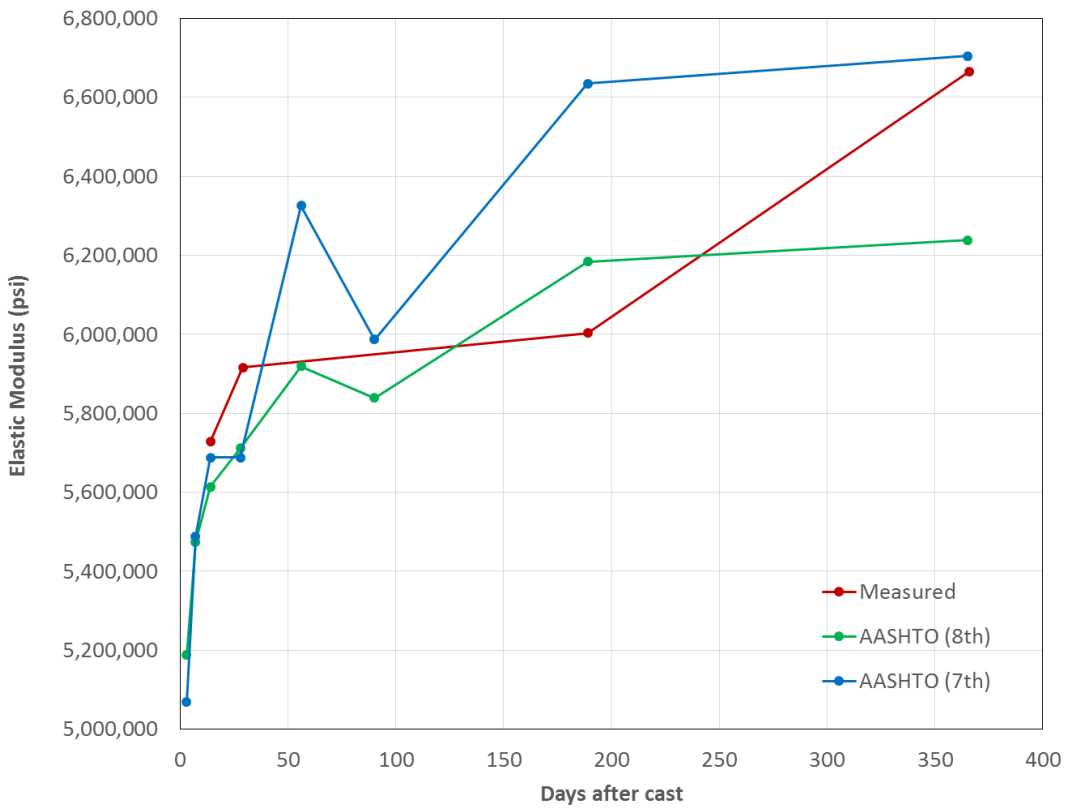

Figure 4-17. Comparison of elastic modulus

4.3 Strain Measurement Results

The indoor and outdoor strain measurements were collected one after the other and at the same time of day in the beginning of the experiment to ensure consistency. The measurements were more susceptible to change within the first few weeks of the concrete curing, and thus collected more frequently. After approximately one month, the project collected measurements twice per day, then after three months, roughly one measurement per week. The ambient temperature and relative humidity were recorded twice, before and after strain measurement, from a standing gauge and averaged. The inner temperature of specimens were collected from thermistors. A summary of the measured data is in Appendix B.

Figure 4-18 shows various strain values related to creep and shrinkage strains. The total strain is the sum of creep strain, initial strain or elastic strain, and shrinkage strain if there is no temperature change. The creep strain consists of basic creep and drying creep strains. The shrinkage strain is the sum of autogenous shrinkage strain and drying shrinkage strain.

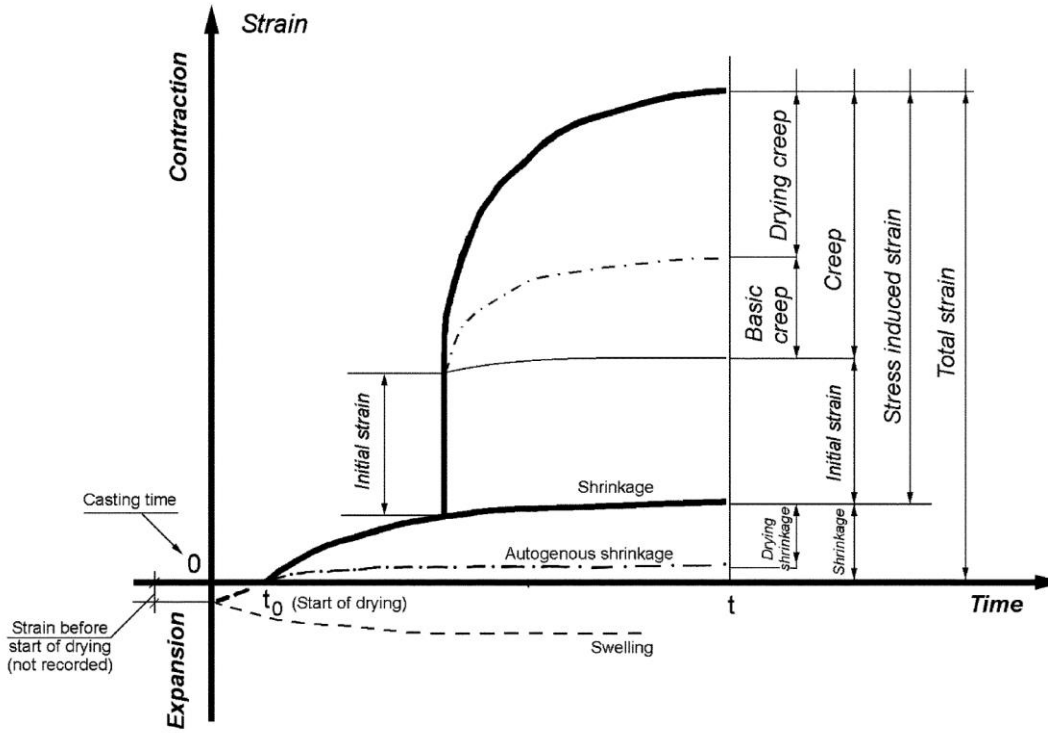

Figure 4-18. Relationship between various measured and derived strain values (ACI 2005)

Following the definition in Figure 4-18, strains measured from the specimens in the creep frames correspond to the total strain, while strains measured from the unloaded specimens are shrinkage strains.

4.3.1 Total Strain Measurement

For each specimen, the project created two measurement lines on opposite sides of the specimen's cylindrical surface and named as Top (T) and Bottom (B). Measurements occurred on each measurement line three times then averaged.

The creep frame placed indoors consisted of specimens V-3 and V-1. Figure 4-19 shows the total strain measured at V-1T (Top measurement line in specimen V-1). The total strain starts at roughly a change of 500$\mu\varepsilon$ to 1000$\mu\varepsilon$ for the first 50 measurements while V-1B starts at roughly a change of 800$\mu\varepsilon$ to 1300$\mu\varepsilon$ in Figure 4-20. The reason why the values differ when it is the same specimen is not completely clear, but it could be due to orientation of the cylinder and uneven loading along its cross section. Figure 4-21 shows the total strain at V-3B ranging from approximately 500$\mu\varepsilon$ to 900$\mu\varepsilon$ for the first 50 measurements, but displays more of a linear trend rather than exponential as expected. Measurement at V-3T was not used due to inconsistent information. The strain changes of the indoor loaded specimens displayed in Figure 4-22 show an overall exponential trend in the beginning of the collected measurements, with a linear trend that tapers out until unloading.

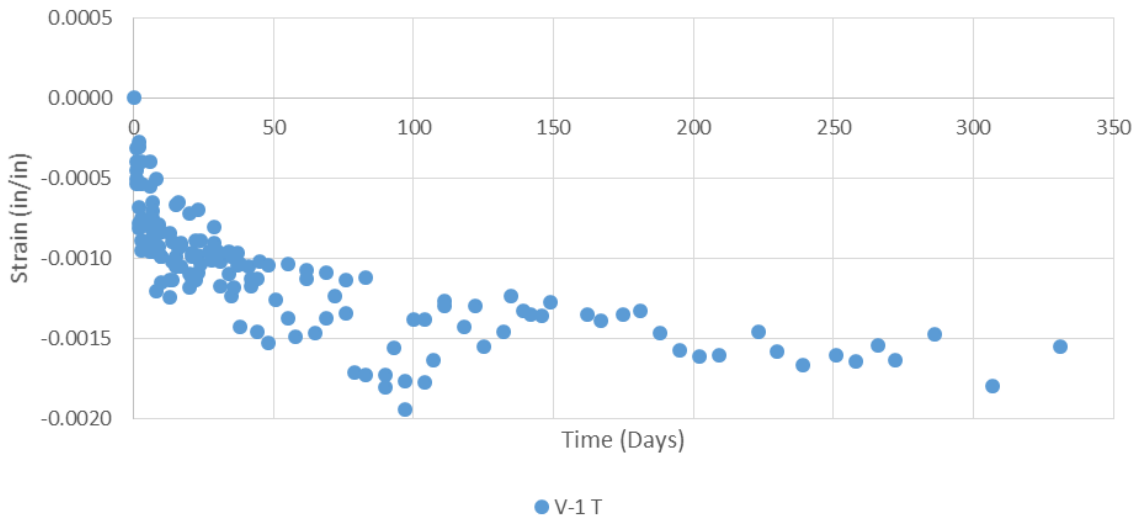

Figure 4-19. V-1 Top (Loaded, Indoor)

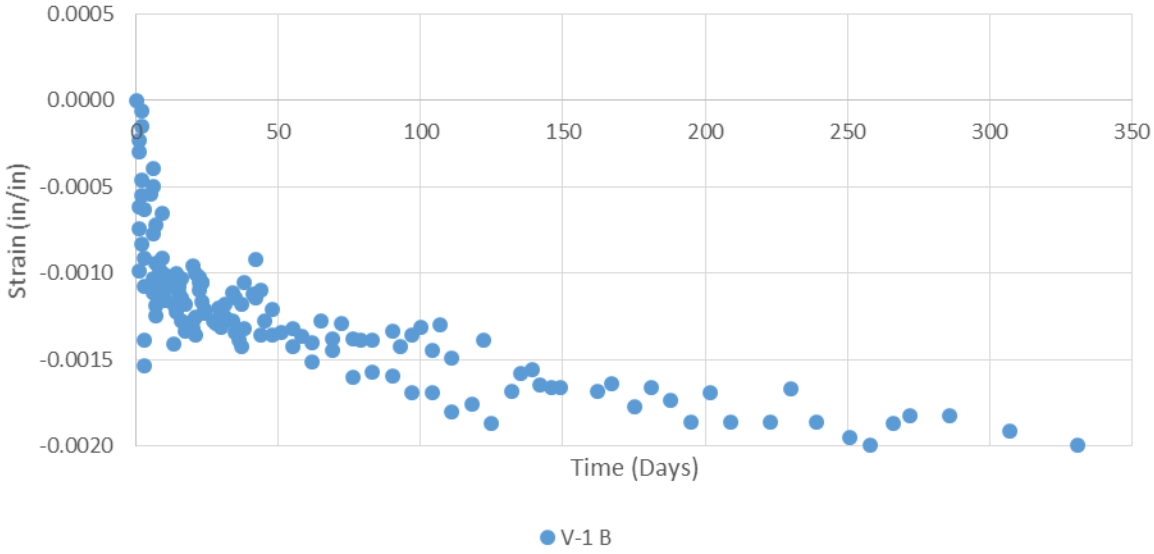

Figure 4-20. V-1 Bottom (Loaded, Indoor)

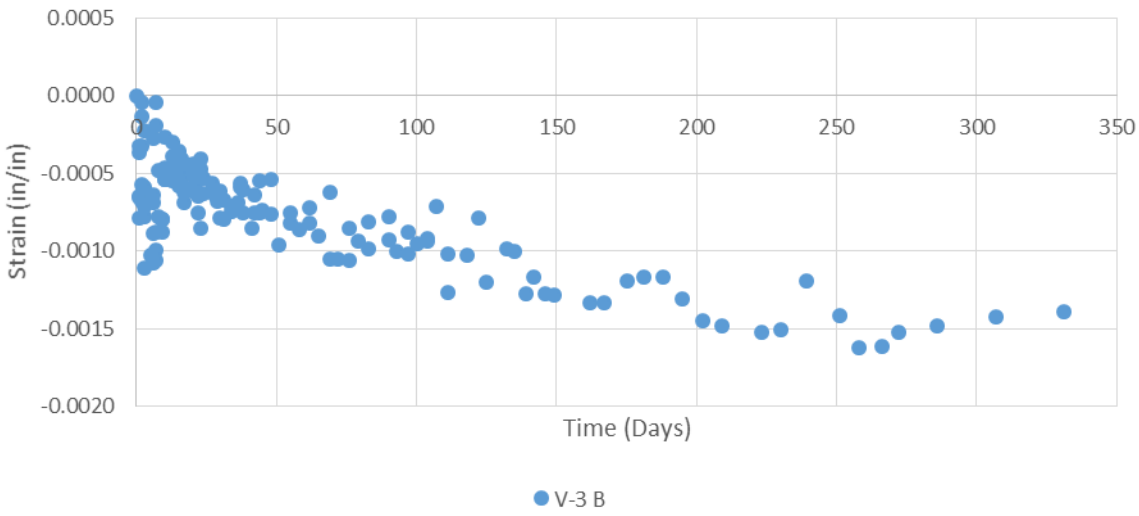

Figure 4-21. V-3 Bottom (Loaded, Indoor)

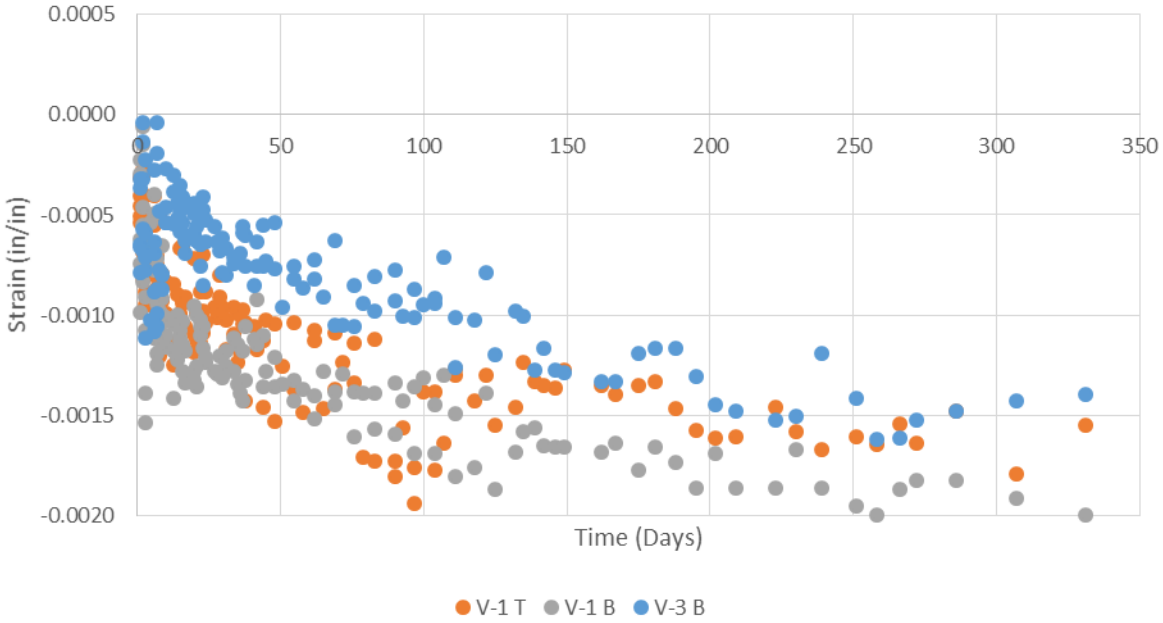

Figure 4-22. Indoor Loaded Strain

Figures 4-23 through 4-26 show the total strain measured from the specimens exposed to the natural environment. Measurement at V-4T in Figure 4-23 shows gradual exponential trend

for the first 100 days with a change of roughly 1,200$\mu\varepsilon$, while specimen V-4B in Figure 4-24 shows a steeper exponential trend with a change of roughly 1,650$\mu\varepsilon$. The other outdoor specimen V-6B in Figure 4-25 shows a similar trend to V-4B with a steep exponential tendency for the first 50 days and tapers out with a change of approximately 1,000$\mu\varepsilon$. The strain changes of the outdoor loaded specimens in Figure 4-26 shows exponential trend for the first 100 days with values from 750$\mu\varepsilon$ to 1,750$\mu\varepsilon$.

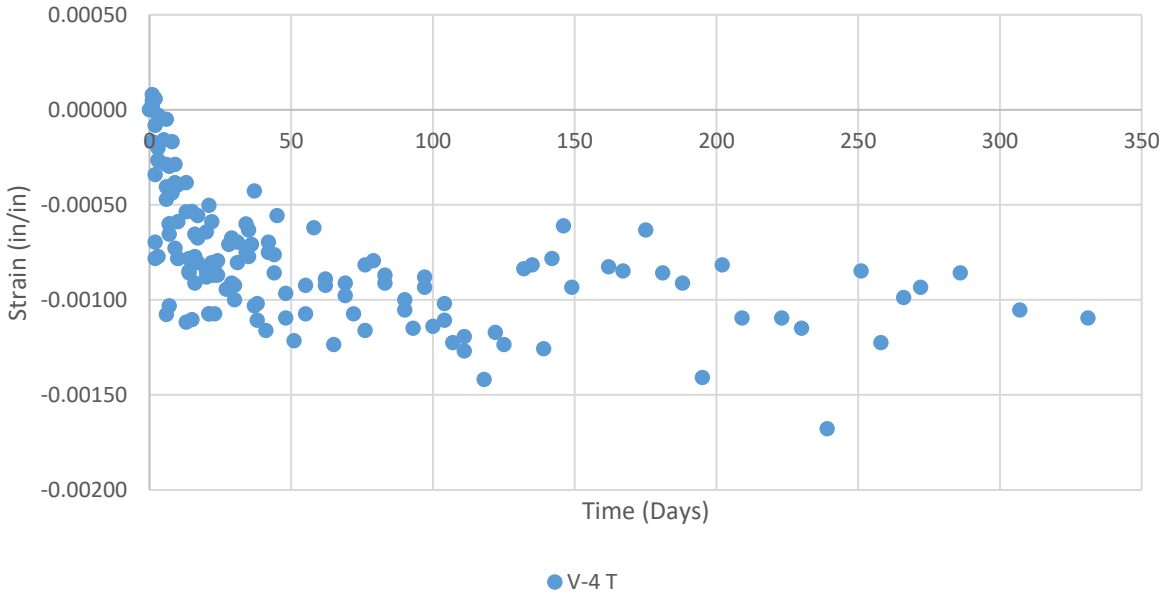

Figure 4-23. V-4 Top (Loaded, Outdoor)

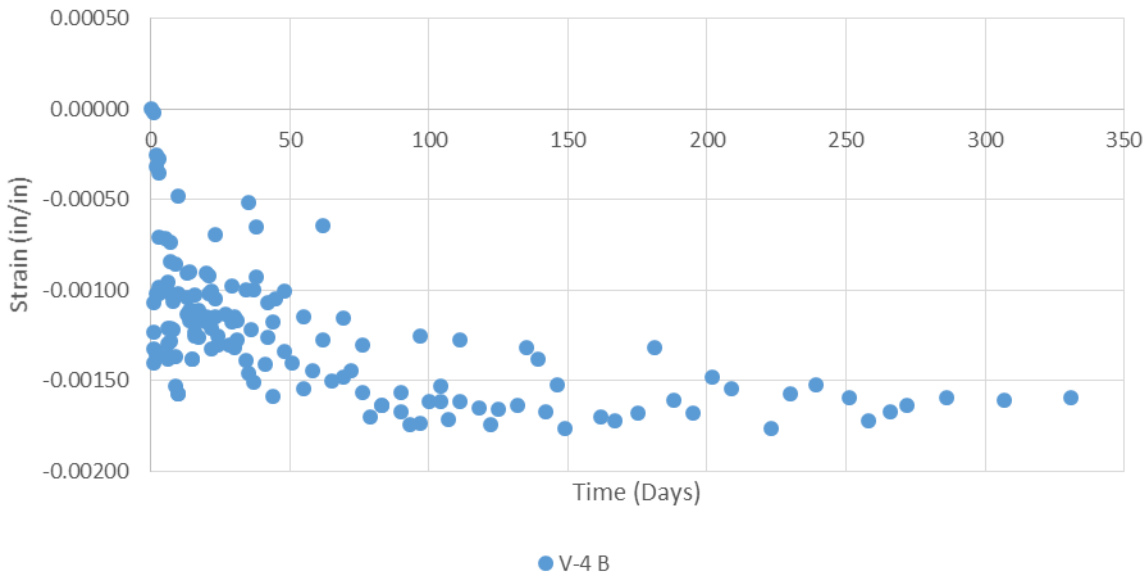

Figure 4-24. V-4 Bottom (Loaded, Outdoor)

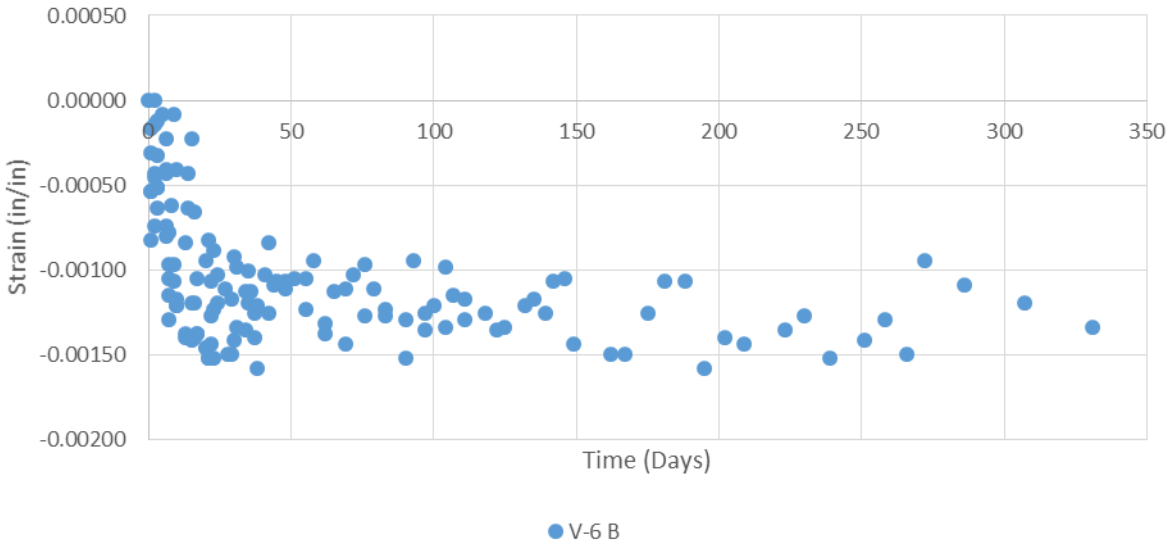

Figure 4-25. V-6 Bottom (Loaded, Outdoor)

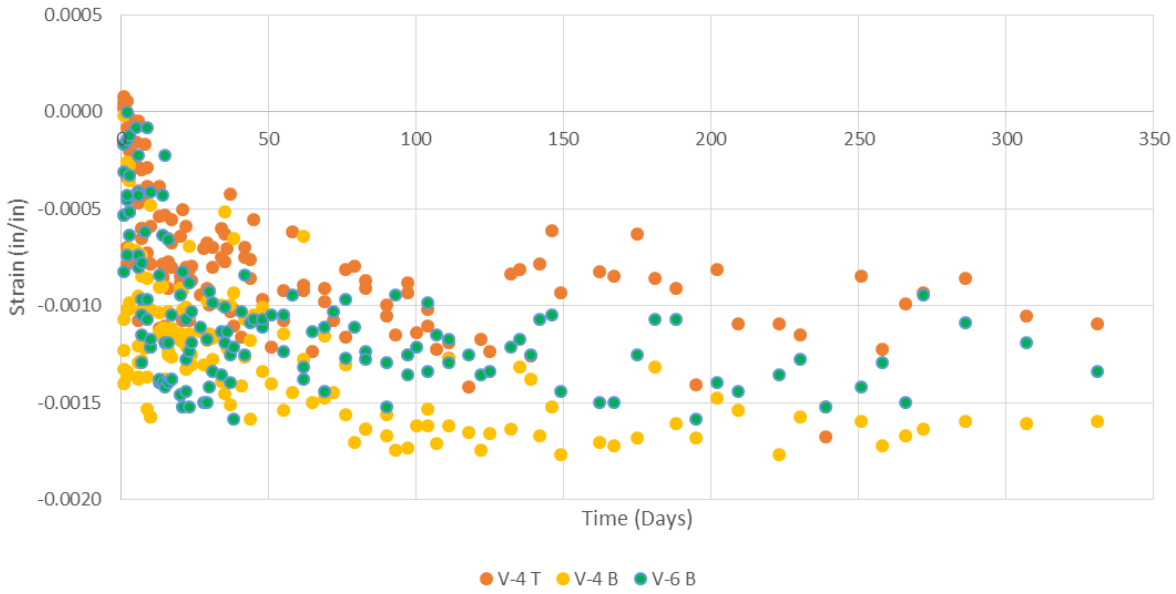

Figure 4-26. All Outdoor Loaded Cylinders

Figures 4-27 and 4-28 show the average of measured total strains from three measurement positions. In addition, a trend line added in each figure shows a different pattern between indoor and outdoor total strains. Between 0 and 50 days after measurement started, the total strains from the outdoor frame were greater than the ones from the indoor frame. Between 50 and 100 days after measurement started, two curves from the two frames are similar in their patterns and values. After 100 days, the total strain from the indoor frame slowly increased reaching 1,600 to 1,700 $\mu\varepsilon$ after 250 days. However, the total strain from the outdoor frame did not change much. They varied between 1,000 and 1,500 $\mu\varepsilon$ and the averaged total strain was 1,300 $\mu\varepsilon$ after 250 days.

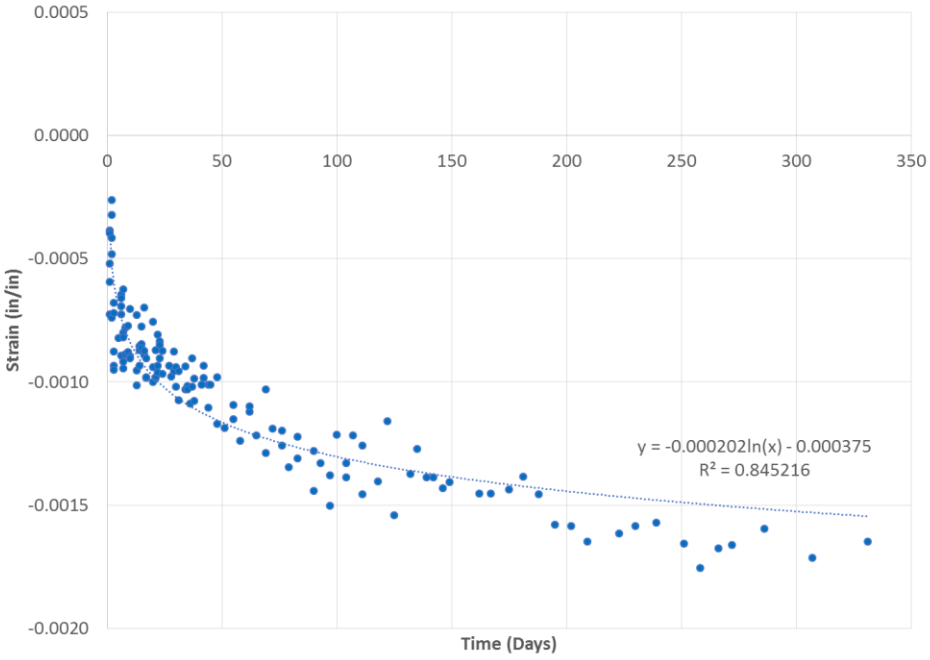

Figure 4-27. Indoor Loaded Comparison

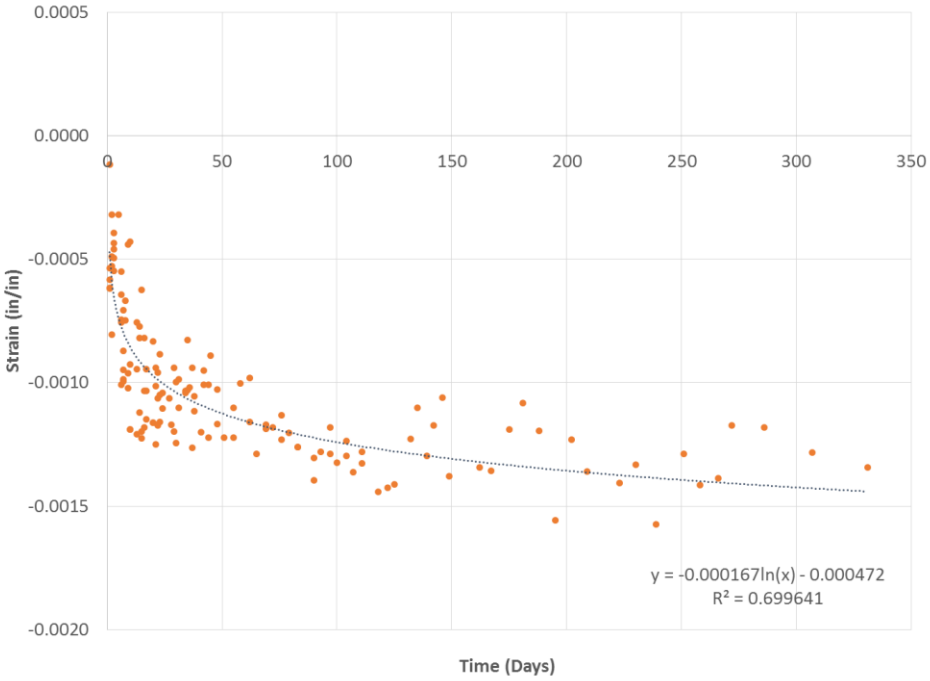

Figure 4-28. Outdoor Loaded Comparison

Figures 4-29 and 4-30 use a logarithmic scale to draw the total strain in the indoor and outdoor frames. A parabolic curve was used to generate a trend line with a constraint of having -0.0005 as a y-intercept which corresponded to the initial strain. Comparison of the two trend lines indicates a different sign the second order term. It is -0.000114 for the indoor frame and it is +0.000016 for the outdoor frame. Thus, the strain increased much greater and faster in the indoor frame than the outdoor frame.

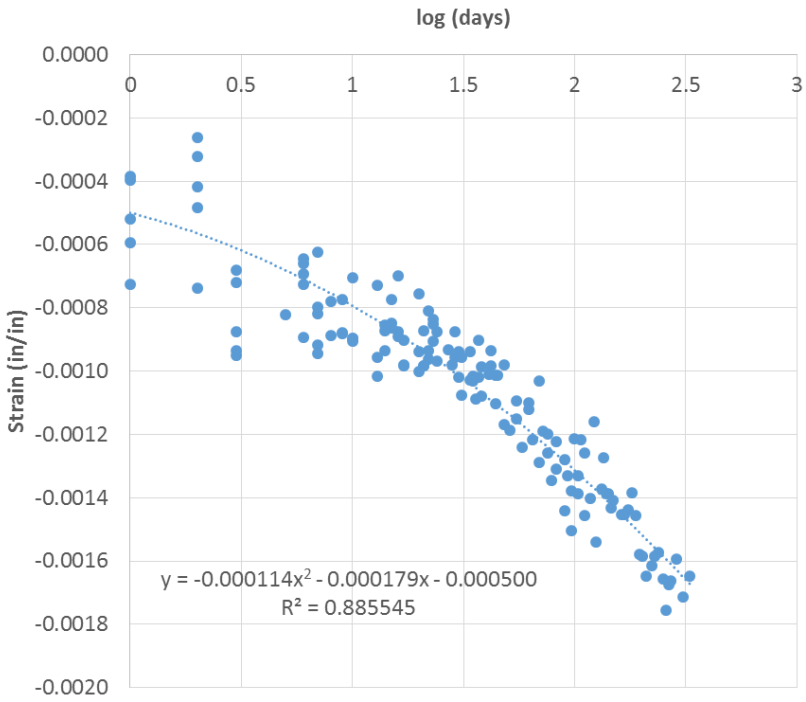

Figure 4-29. Indoor Total Strain in log(days)

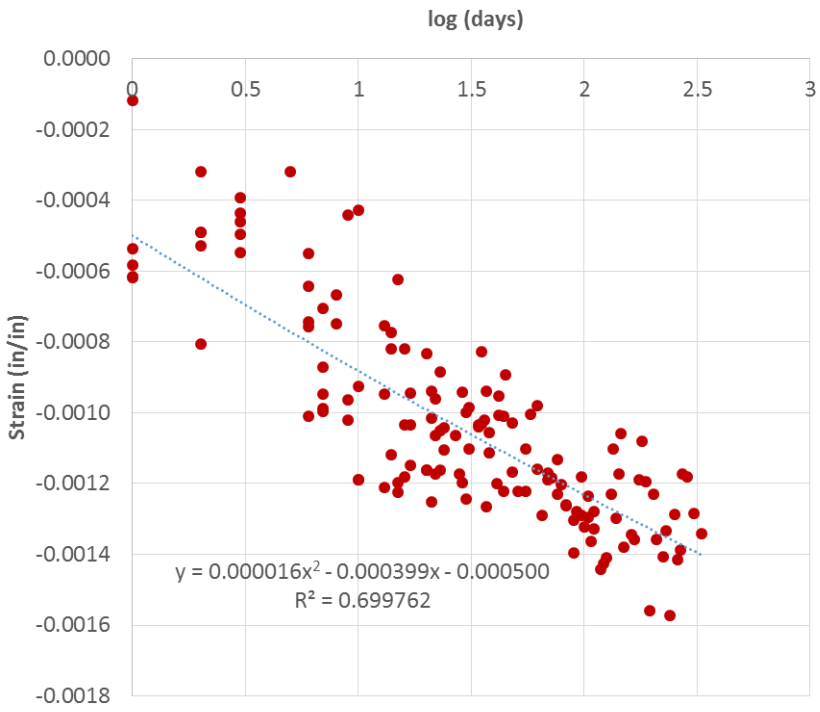

Figure 4-30. Total Strain in log(days)

4.3.2 Shrinkage Measurements

The project measured shrinkage strains from two unloaded specimens for each frame. The specimens were the same in size as the loaded cylinders and located next to the indoor and outdoor frames. The shrinkage strain from indoor specimens shown in Figure 4-31, demonstrates a change of roughly 500$\mu\varepsilon$ in the first 50 days, then a steadily increasing trend until measurements stop at a maximum of 1000$\mu\varepsilon$. The outdoor specimens in Figure 4-32 show a similar trend within the first 50 days at roughly 500$\mu\varepsilon$, however, the data does not steadily increase like the indoor specimens after this point but tapers off until no change can be seen. This long term effect of shrinkage may be due to the weather outdoors varying between warm and

cold, while the indoor specimens did not fluctuate. In order to verify this effect the temperature and relative humidity of the ambient air and the inside the specimens must be analyzed.

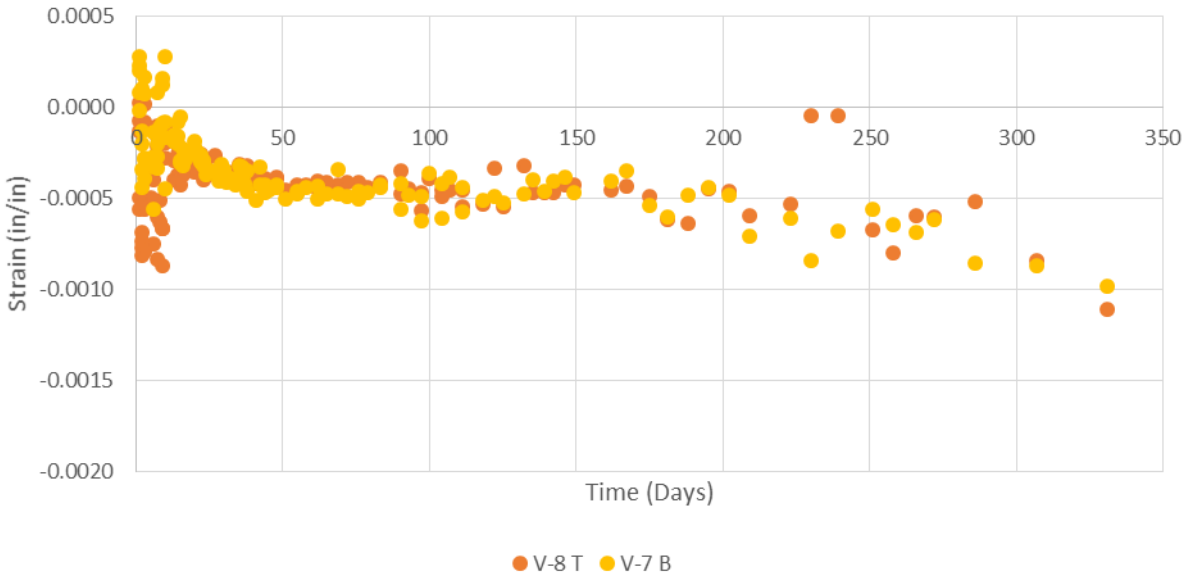

Figure 4-31. Indoor Unloaded Strain

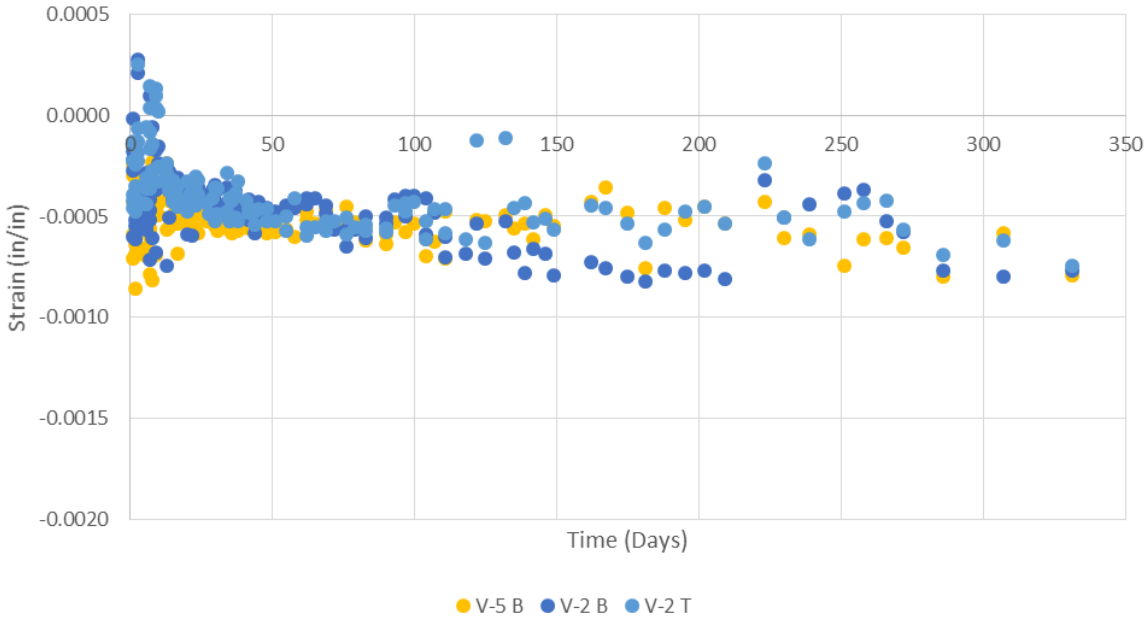

Figure 4-32. Outdoor Unloaded Strain

4.3.3 Temperature and Relative Humidity Data

Temperature and relative humidity are the factors identified as the main causes of concrete creep and shrinkage, as the concrete has not yet fully hardened before exposure to non-ideal environments (ACI 2008). For the indoor specimens, a digital weather station measured the ambient temperature and relative humidity. The project recorded measurements before and after the creep and shrinkage measurements. The thermistor installed in specimens monitored the internal temperature. Figure 4-33 shows the ambient temperature and internal temperature measured for the entire period. The room maintained a relatively uniform temperature with the average ambient temperature at roughly 22.4°C and the average internal temperature at 22.67°C. Figure 4-34 compares the change of relative humidity with the average total. It shows that the air was dry for the time of the test, and it became very dry between days 100 and 331. The average relative humidity of this period was 8.9%.

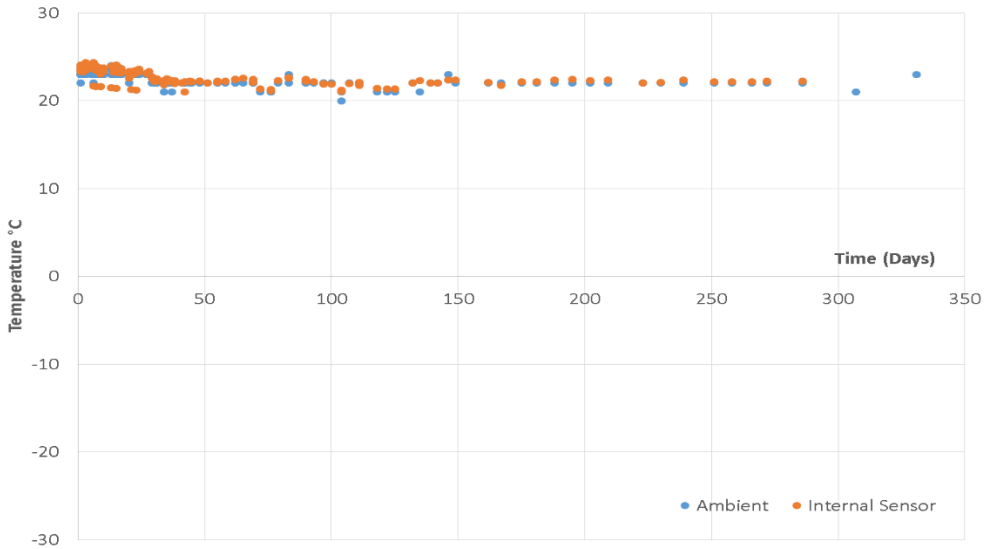

Figure 4-33. Indoor Measured Temperature

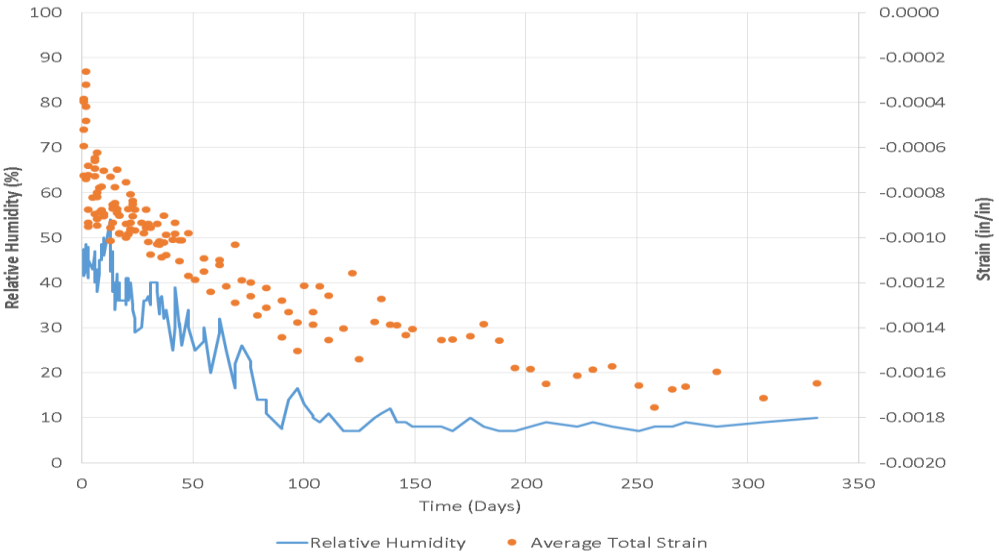

Figure 4-34. Indoor Relative Humidity and Strain Comparison

Figure 4-35 shows the three types of temperature collection for the outdoor specimens: a weather station on the Elvey Building (Meso West) on West Ridge of the UAF Campus, an internal sensor, and an onboard weather station to collect ambient air temperature. From the figure it can be seen that the natural swing from higher to lower to higher temperatures reveals a full season with a high of roughly 28°C and a low of -30°C. Due to daily temperature fluctuation, it can be seen that the three temperature readings varied. Specifically, the difference is substantial when the temperature dropped below 0°C in days 100 and 250.

Figure 4-35 shows the change of relative humidity. The average total strain included for comparison. Between days 100 and 250, the relative humidity became high, and the overall change of the total strain became small. This comparison shows that the total strain in the outdoor frame became smaller partially due to high relative humidity during the winter season.

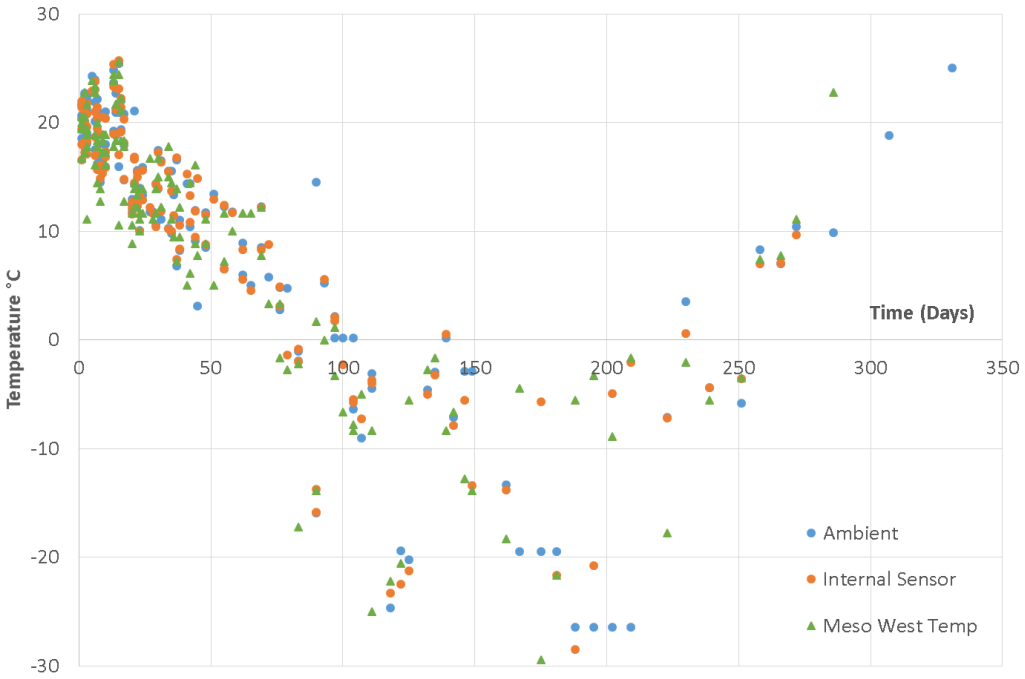

Figure 4-35. Outdoor Measured Temperature

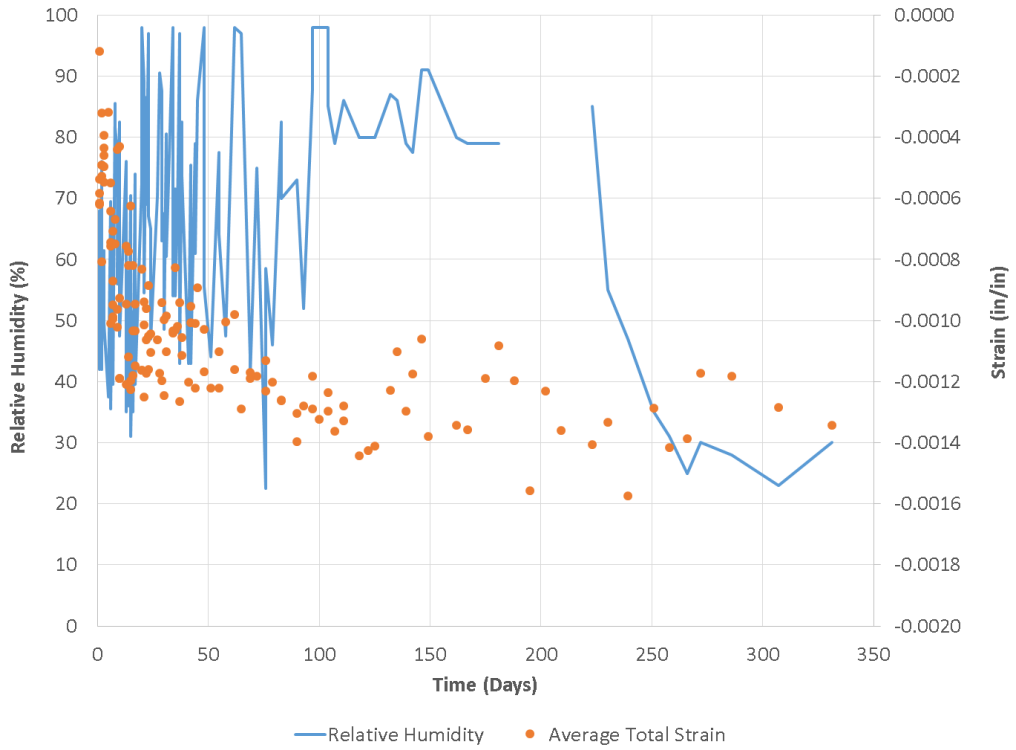

Figure 4-36. Outdoor Relative Humidity and Strain Comparison

CHAPTER. 5 DESIGN IMPLICATION

The project compared the measured total strains with predicted values from several shrinkage and creep models. It used models ACI 209R-92, Bažant-Baweja B3, CEB MC90-99, and GL 2000 from ACI 209.2R-08 (ACI 2008). In addition, the models used in the AASHTO LRFD were included for comparison (AASHTO 2017). The researchers used the model that best fit the measured data to predict pre-stress losses.

5.1 Concrete Shrinkage and Creep Models

While shrinkage and creep may vary with local conditions, research has shown that short-term shrinkage and creep measurements improve the predictions regardless of location (Bažant 1987, Bažant and Baweja 2000, Aguilar 2005). For this reason, the ACI committee recommends short-term testing to determine the shrinkage, creep, and elastic modulus of the concrete to improve the predictions of the long-term deformations of the concrete.

The collection of shrinkage and creep data from around the world was initially done by Bažant and Panula and placed in a databank, which was then extended by the ACI and CEB. The issues with the databank include but are not limited to which data sets are included, the description of the concrete, European cement concretes versus United States, and experiments using smaller specimens. Several models, compromising between accuracy and convenience, have been proposed for the prediction of creep, drying shrinkage, and total strains under load. The user-friendly modeling includes specifications of the concrete to make a prediction such as its age at loading, ambient relative humidity, duration of loading, specimen size, among others. The ACI committee recognized that the stiffness of the aggregate significantly affects the

shrinkage and creep of concrete (ACI 2008). Some models account for this effect while others use concrete strength as an adjustment. If no mechanical characteristics of the concrete are available, relying solely on concrete mix information may not account for the behavior due to aggregate properties.

Various models were selected to be used for comparison, mainly; the ACI 209R-92 (ACI 1992), the Bažant-Baweja B3 model developed by Bažant and Baweja (1995, 2000), the CEB Model Code 1990-99 (CEB MC90-99)(Muller and Hillsdorf 1990, CEB 1999), and the GL2000 model developed by Gardner and Lockman (2001). The comparison of the various models using experimental data complicates the result, showing lack of agreement on selection of the appropriate data and on the method used to compare the correlation. Table 5-1 lists the individual model's applicable range for different input variables.

Table 5-1. Parameter Ranges of Each Model

Input variables	Model				
	ACI 209R-92	Bažant-Baweja B3	CEB MC90	CEB MC90-99	GL2000
f_{cm28}, MPa (psi)	—	17 to 70 (2500 to 10,000)	20 to 90 (2900 to 13,000)	15 to 120 (2175 to 17,400)	16 to 82 (2320 to 11,900)
a/c	—	2.5 to 13.5	—	—	—
Cement content, kg/m^3 (lb/yd^3)	279 to 446 (470 to 752)	160 to 720 (270 to 1215)	—	—	—
w/c	—	0.35 to 0.85	—	—	0.40 to 0.60
Relative humidity, %	40 to 100	40 to 100	40 to 100	40 to 100	20 to 100
Type of cement, European (U.S.)	R or RS (I or III)	R, SL, RS (I, II, III)	R, SL, RS (I, II, III)	R, SL, RS (I, II, III)	R, SL, RS (I, II, III)
t_c (moist cured)	≥ 1 day	≥ 1 day	< 14 days	< 14 days	≥ 1 day
t_c (steam cured)	1 to 3 days	—	—	—	—
t_o	≥ 7 days	$t_o \geq t_c$	> 1 day	> 1 day	$t_o \geq t_c \geq 1$ day

5.1.1 ACI 209R-92 Model

The ACI Committee 209R-92 developed a prediction model of creep, shrinkage, and temperature effects in concrete structures (ACI 2008). Their method concerns normal weight concrete having a compressive strength of 6,000psi or less. However, the methodology still applies to high strength concrete with a compressive strength greater than 6,000psi. The advantages of this model include its simplicity, and the model is relatively easy to adjust to match short-term test data. The disadvantages include its limitations in accuracy when accommodating member size. The model is empirical, not based on shrinkage or creep phenomena. The required input values are only age of concrete when drying starts, age of concrete at loading, curing method, relative humidity expressed as a decimal, volume-surface ratio, and cement type. The model does not calculate compliance but calculates the creep coefficient, which may introduce problems with an assumed value for elastic modulus. The formula for shrinkage time function and shrinkage strain are in Equations 5-3 and 5-4,

$$f(t,t_c) = \left[\frac{(t-t_c)^{\alpha}}{(f+(t-t_c)^{\alpha})}\right] \tag{5-3}$$

$$\varepsilon_{sh}(t,t_c) = \frac{(t-t_c)^{\alpha}}{f+(t-t_c)^{\alpha}}\,\varepsilon_{shu} \tag{5-4}$$

where

ε_{shu} = ultimate shrinkage strain

α = air content expressed as percentage

f = number of days

The variables f and α, are considered constants for a given member shape and size. The creep coefficient time function and the creep coefficients are shown in Equations 5-5 and 5-6,

$$f(t-t_0) = \left[\frac{(t-t_0)^{\Psi}}{(d+(t-t_0)^{\Psi})}\right] \quad (5\text{-}5)$$

$$\phi(t,t_0) = \left[\frac{(t-t_0)^{\Psi}}{(d+(t-t_0)^{\Psi})}\right]\phi_u \quad (5\text{-}6)$$

where

ϕ_u = ultimate shrinkage strain

γ_c = unit weight of concrete

Ψ = fine aggregate percentage

d = number of days

5.1.2 Bažant-Baweja B3 Model

The Bažant-Baweja B3 model is the latest variant in a number of shrinkage and creep prediction methods developed. This current model derives from a simpler and more theoretically justified version than previous models, based on a mathematical description of over 10 physical phenomena affecting creep and shrinkage (Bažant 2000). This particular model is useful for those dealing with complex as well as simple structures. The compliance function is utilized to reduce the risk of errors due to inaccurate values of the elastic modulus. The factors taken into account include age of concrete when drying starts, age of concrete at loading, aggregate and cement content, cement type, concrete mean compressive strength at 28 days, curing method,

relative humidity, shape of specimen, volume-surface ratio, and water content in concrete. The mean shrinkage strain and shrinkage time function are calculated by Equations 5-7 and 5-8,

$$\varepsilon_{sh}(t, t_c) = -\varepsilon_{sh\infty} k_h tanh\left[\frac{(t-t_c)}{\tau_{sh}}\right]^{0.5} \quad (5\text{-}7)$$

$$S(t - t_c) = tanh\left[\frac{(t-t_c)}{\tau_{sh}}\right]^{0.5} \quad (5\text{-}8)$$

where

t = age of concrete (days)

t_c = start of drying (days)

$\varepsilon_{sh\infty}$ = ultimate shrinkage strain

k_h= ambient relative humidity factor

$S(t - t_c)$ = the time curve

$(t - t_c)$ = the time from the end of the initial curing

τ_{sh} = shrinkage half time given in days

The compliance function for basic creep is given by Equation 5-9,

$$C_0(t, t_0) = q_2 Q(t, t_0) + q_3 ln[1 + (t - t_0)^n] + q_4 ln\left(\frac{t}{t_0}\right) \quad (5\text{-}9)$$

where

q_2 = aging viscoelastic term

q_3 = non-aging viscoelastic term

q_4 = aging flow term

$Q(t,t_0) = Q_f(t_0)\left[1 + \left\{\frac{Q_f(t_0)}{Z(t,t_0)}\right\}^{r(t_0)}\right]^{\frac{-1}{r(t_0)}}$ = aging viscoelastic term Part 1

$Z(t,t_0) = (t_0)^{-m} ln[1 + (t - t_0)^n]$ = aging viscoelastic term Part 2

m = Constant = 0.5

n = Constant = 0.1

$r(t_0)$ = Constant = 10.333

$Q_f(t_0)$ = Constant = 0.246

5.1.3 CEB MC90-99 Model

The CEB MC90-99 model is a revised version that takes into account both normal and high-strength concrete. In terms of creep and shrinkage-sensitive structures, this method is more widely used than the ACI 209R-92 model. However, the correction term used for relative humidity in the creep equation is extremely sensitive to any variation in relative humidity. This method requires the age of concrete when drying starts and at loading, concrete mean compressive strength at 28 days, relative humidity, volume-surface ratio, and cement type.

Note that European models were considered when optimizing this model, meaning that the model underestimates the shrinkage of North American concretes, and substantially underestimates the shrinkage of concretes containing basalt aggregates (ACI 2008). The shrinkage strain and shrinkage time function are calculated by Equations 5-10 and 5-11,

$$\varepsilon_{sh}(t,t_c) = \varepsilon_{cso}\beta_s(t - t_c) \quad (5\text{-}10)$$

$$\beta_s(t-t_c)=\left[\frac{\left\{\frac{(t-t_c)}{t_1}\right\}}{\left\{350\left[\frac{\left(\frac{V}{S}\right)}{\left(\frac{V}{S}\right)_0}\right]^2+(t-t_c)/t_i\right\}}\right]^{0.5} \quad (5\text{-}11)$$

where

ε_{cso} = notional shrinkage coefficient

$\frac{V}{S}$ = volume to surface ratio

$(t-t_c)$ = duration of drying (days)

The creep coefficient and creep coefficient time function are calculated by Equations 5-12 and 5-13,

$$\phi_{28}(t,t_0)=\phi_0\beta_c(t-t_c) \quad (5\text{-}12)$$

$$\beta_c(t-t_0)=\left[\frac{\frac{(t-t_0)}{t_1}}{\left\{\beta_H+\frac{(t-t_0)}{t_1}\right\}}\right]^{0.3} \quad (5\text{-}13)$$

where

β_H = relative humidity adjustment factor

ϕ_0 = notional shrinkage coefficient

t_0 = age of loading

5.1.4 GL2000 Model

The GL2000 model developed by Gardner and Lockman (2001) is a modification made to conform to the ACI 209 model guidelines. The model is convenient to use because other than compressive strength, it only requires input data that are available to the engineer at time of design. The method requires the age of the concrete when drying starts and when it is loaded, relative humidity, volume-surface ratio, cement type, and concrete mean compressive strength at 28 days. The shrinkage strain and shrinkage time function are calculated by Equations 5-14 and 5-15,

$$\varepsilon_{sh}(t, t_c) = \varepsilon_{shu}\beta(h)\beta(t - t_c) \tag{5-14}$$

$$\beta(t - t_c) = \left[\frac{(t-t_c)}{\left\{t-t_c+77\left(\frac{V}{S}\right)^2\right\}}\right]^{0.5} \tag{5-15}$$

where

ε_{shu} = ultimate shrinkage strain

$\beta(h)$ = ambient relative humidity factor

The basic creep coefficient is calculated by Equation 5-16,

$$\phi_{28}(t, t_0) = 2\left[\frac{(t-t_0)^{0.3}}{\{((t-t_0)^{0.3}+14)\}}\right] + \left[\frac{7}{t_0}\right]^{0.5}\left[\frac{(t-t_0)}{\{(t-t_0)+7\}}\right]^{0.5} \tag{5-16}$$

5.1.5 AASHTO LRFD Model

The AASHTO LRFD model formed a basis for calculation since it is the model used for bridge design. The shrinkage is calculated using Equation 5-17 while the creep coefficient and compliance derive from Equations 5-18 and 5-19 as follows;

$$\varepsilon_{bid} = k_{shape} * k_{hs} * k_f * k_{eva} * 48 * 10^{-3} \quad (5\text{-}17)$$

$$\psi_{creep} = 1.9 * k_{shape} * k_{hc} * k_f * k_{eva} * t_{ini}^{-0.118} \quad (5\text{-}18)$$

$$J_{t,t_0} = J_{t_0,t_0} + \frac{\psi_{creep}}{E_{cmto}} \quad (5\text{-}19)$$

where

k_{shape} = volume-surface factor

k_{hc} = humidity factor for creep

k_{hs} = humidity factor for shrinkage

k_f = concrete strength factor

k_{eva} = time development factor

t_{ini} = age at loading

E_{cmto} = measured mean elastic modulus

5.1.6 Model Comparison

The project used five models to predict the total strain of the indoor and outdoor frames. The total strains were calculated from the loading day (14 day) to 365 day based on the measured material properties. All required parameters used in the models were from the concrete mix

design document and test results in the present study. Table 5-2 shows selected material properties used in the models.

Table 5-2. Selected Parameters in the Models

Parameter	Value	Remark
unit weight of concrete	$\gamma_c = 152\,pcf$	concrete mix document
Concrete compressive strength	$f_c^{'} = 8000\,psi$	specified 28day strength
	$f_{c\_14d}^{'} = 8654\,psi$	measured 14day strength
	$f_{c\_28d}^{'} = 9119\,psi$	measured 28day strength
Elastic modulus	$E_{c\_14d} = 5727643\,psi$	measured 14day modulus
	$E_{c\_28d} = 5915679\,psi$	measured 28day modulus
Relative humidity	*RH=0.4*	Indoor frame
	RH=0.686	Outdoor frame
Volume-surface ratio	*1.3 in.*	6″×12″ cylinder
Stress applied	$f_{start} = 2829\,psi$	initial load (80kips)
	$f_{end} = 2476\,psi$	final load (70kips)

Figure 5-1 shows the total strains calculated from the models with measured total strains for the indoor frame. A relative humidity of *RH=0.4* and an applied stress of $f_{start} = 2829\,psi$ are used in the models. The ACI model has values exceeding the others until day 50, showing that it is more sensitive in short term shrinkage measurements indoors. It is also noted that in the shrinkage comparison the values until day 28 are zero for all except the GL2000, this is because the difference in the age of concrete at loading being 7 days versus 28 days. For shrinkage strains, after the initial changes settle out, the models seem to have a similar trend line over long terms, except the GL2000 with a slightly steeper trend. The measured total strains match well

with the CEB MC90-99 model. The AASHTO LRFD model has the smallest slope so that long-term prediction from this model is substantially smaller than other models.

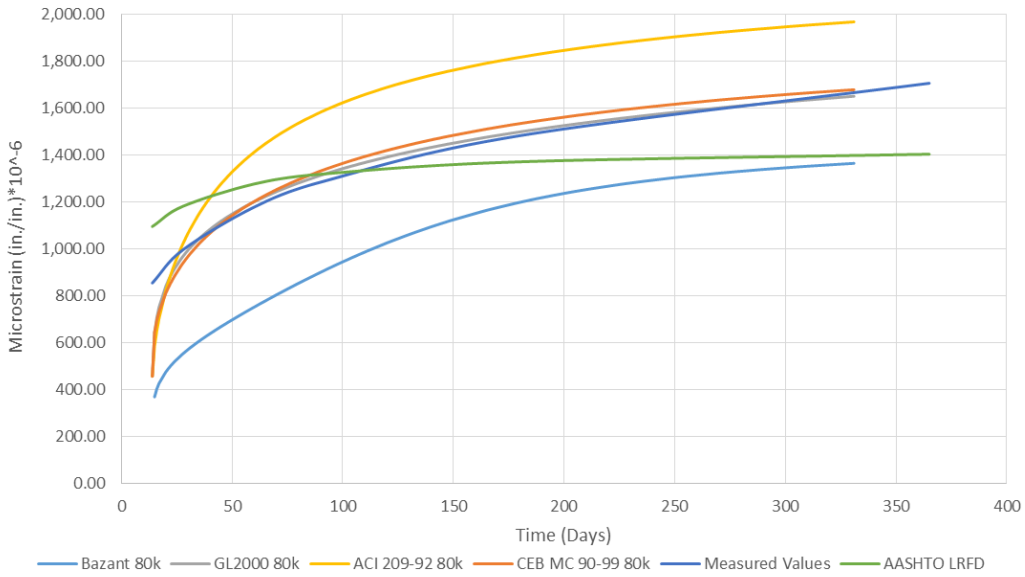

Figure 5-1. Total Strain Comparison (Indoor, 80kip)

Figure 5-2 compares the total strains from the models with the measured strains. A relative humidity of *RH=0.686* and an applied stress of $f_{start} = 2{,}829\,psi$ are used in the models. The Bažant-Baweja B3 model underestimated strains while the GL2000 model shows a closer trend as time goes on. The ACI 209-92 and GL2000 models predicted strains closer to the measured strains, which are seen as a more conservative estimation in short term. Specifically, the measured total strains match well with the ACI 209-92 model in a wide range.

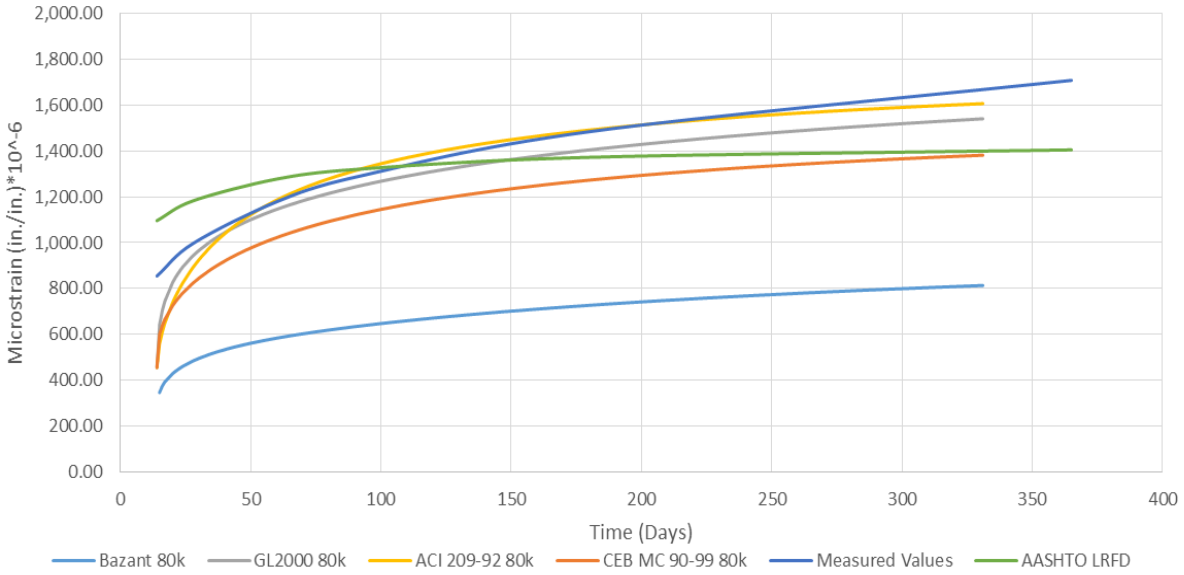

Figure 5-2. Total Strain Comparison (Outdoor, 80kip)

Figures 5-3 and 5-4 represent the range of 70k to 80k that each model predicts, to show the range of measured values during testing.

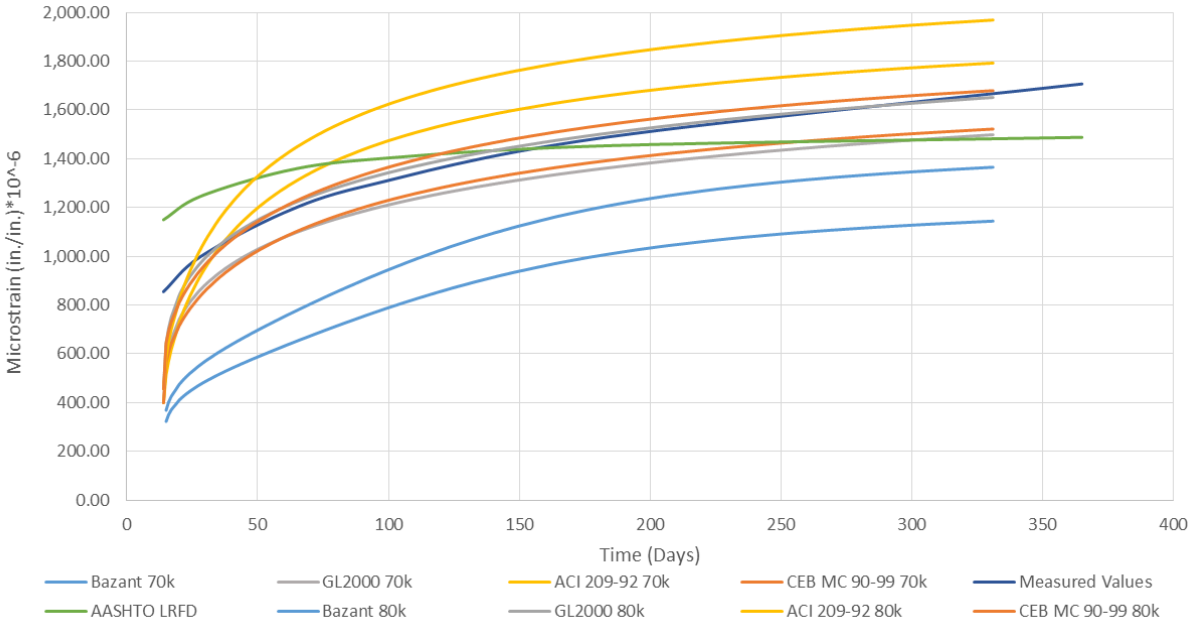

Figure 5-3. Total Strain Comparison (Indoor, 80 kip+70 kip)

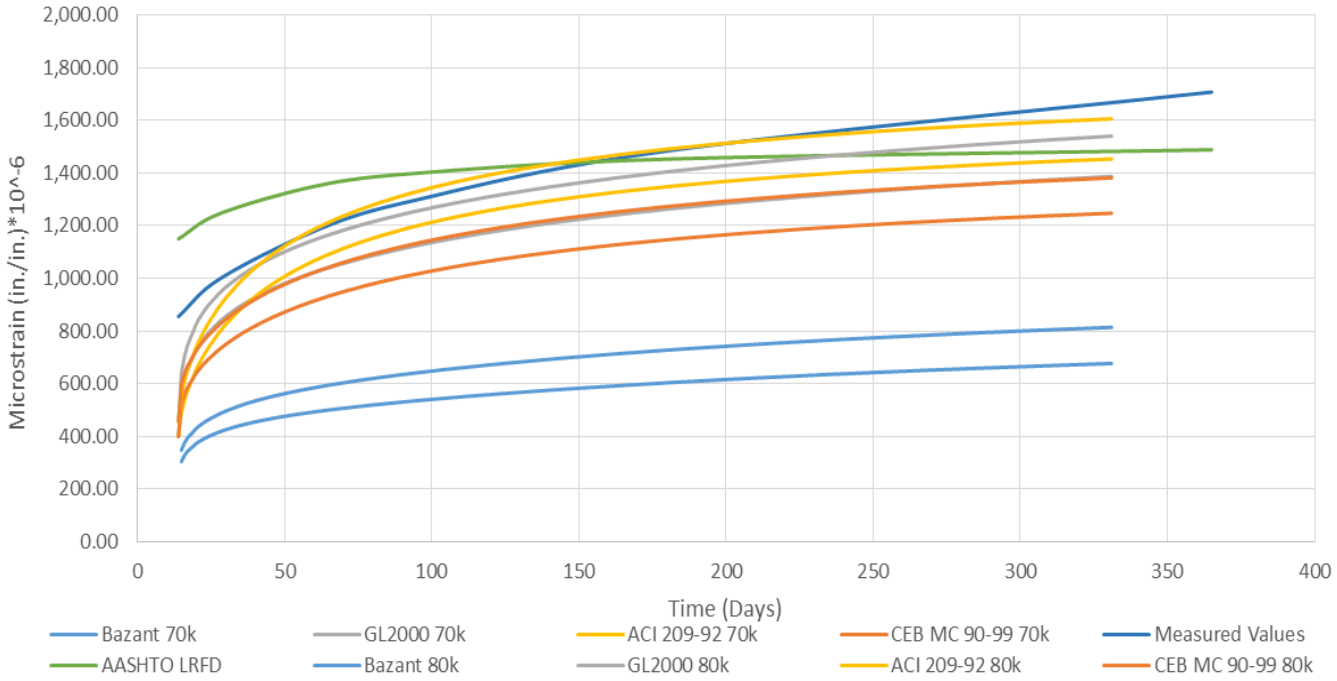

Figure 5-4. Total Strain Comparison (Outdoor, 80 kip+70 kip)

Figures 5-5 and 5-6 estimate total strains for the entire 75-year design life expectancy of a DBT bridge girder. The relative humidity values are 0.4 and 0.686, respectively, and the applied stress is $f_{start} = 2829 psi$ for both. Excluding the AASHTO LRFD model prediction, it reveals that the indoor comparison ranges from approximately 2,000 to 3,100 micro strain, while the outdoor comparison ranges from approximately 1,600 to 2,300 micro strain. It should be noted that the CEB MC90-99 model was the best fit with the measured data for 365 days, and it was the ACI 209-92 model for the outdoor frame case.

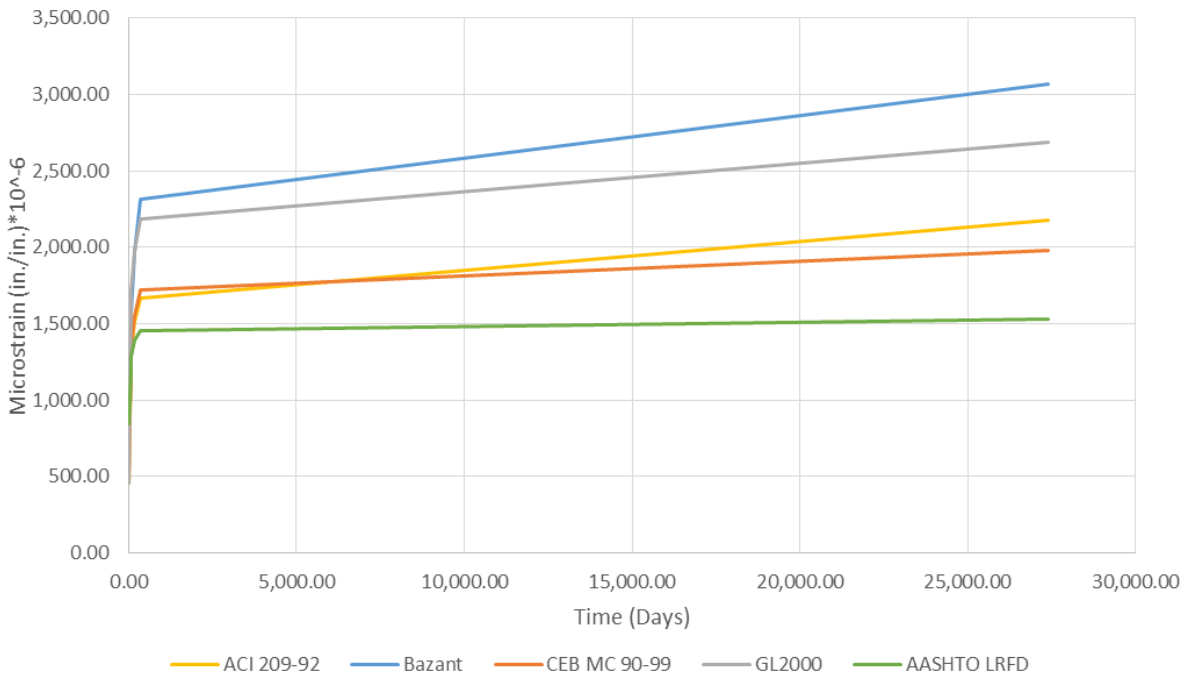

Figure 5-5. Indoor 75-year Prediction Model Comparison

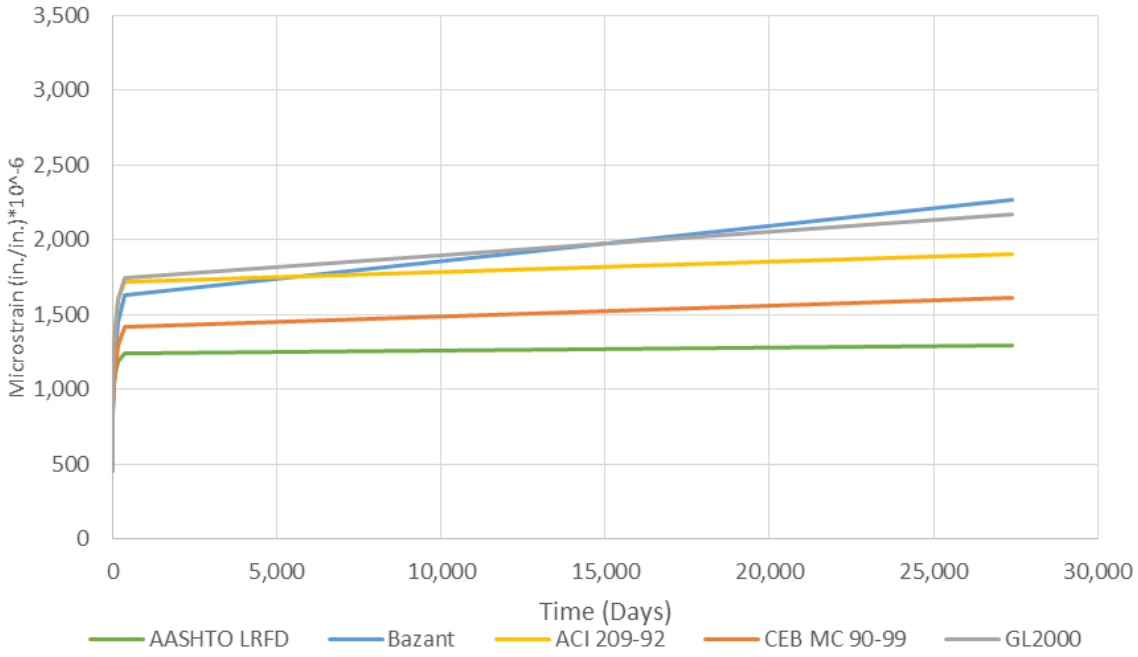

Figure 5-6. Outdoor 75-year Prediction Model Comparison

5.2 Comparison of Time-Dependent Pre-Stress Losses

In this section, the time-dependent pre-stress losses are calculated and compared. The time-dependent pre-stress losses are results from concrete creep, concrete shrinkage, and relaxation of strands. Specifically, pre-stress losses from the following three methods are compared:

- 2004 AASHTO LRFD Lump-Sum method.
- 2017 AASHTO LRFD Refined Estimation.
- 2017 AASHTO LRFD Refined Estimation with a modification of creep coefficient and shrinkage from the ACI 209-92 model.

From the comparison with measured total strains, the ACI 209-92 model was the best match for the outdoor frame. Therefore, the 2017 AASHTO LRFD model concrete creep coefficients replaced those from the ACI 209-92 model is the last method listed above.

The overall pre-stress loss estimation must utilize the specific structures properties in terms of geometry. Thus, the section properties of the Tulsona Creek DBT Girder in Figure 5-7 were used in the calculation. In addition, Table 5-3 shows major input parameters used in pre-stress loss prediction.

Part	Shape	Height	Width	Ai	yi	Aiyi	I I'	Ai di2	Perimeter length
		in	in				in^4	in^4	in
A	SQ	6.0	66.4	398.3	63.0	25089.8	1194.75	167068.70	78.38
B	SQ	60.0	6.0	360.0	30.0	10800.0	108000.00	56413.27	96.00
C	SQ	1.0	43.0	43.0	59.5	2558.5	3.58	12400.51	2.00
D	TR	3.0	39.0	58.5	58.0	3393.0	29.25	14021.77	39.46
E	SQ	3.0	4.0	12.0	57.5	690.0	9.00	2693.48	0.00
F	TR	2.0	4.0	4.0	55.3	221.3	0.89	656.92	5.66
G	TR	3.0	19.0	28.5	7.0	199.5	14.25	35953.82	19.92
H	SQ	6.0	19.0	114.0	3.0	342.0	342.00	178031.79	31.00
			Sum	1018.25		43294.08	109593.72	467240.26	272.42
					y_bar	42.52	from the bottom		
					I_g	576833.98			

Ap 0.153 in^2

Group	number of strands	CGS	
	ni	in	ni yi
Harped	36	7	252
Straight	28	3.625	101.5
Sum	64		353.5
CGS	5.523	in	from the bottom

Girder

length	1734	in
Section A	1018.25	in^2
Volume	1765645.5	in^3
Side S	472368.568	in^2
End S (two)	2036.5	in^2
Total S	474405.068	in^2

	number	section	per girder	
		in^2	lb/ft	
Rail support	2	180	54.64	
	number	volume	per girder	
		in^3	lb	lb/ft
diaphragm	6	25803	1958.263	13.552

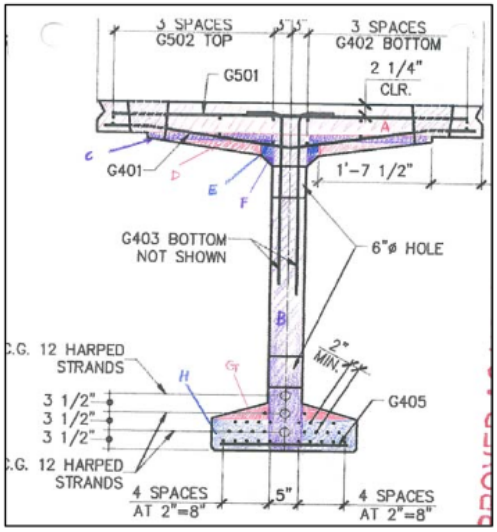

Figure 5-7. Section Properties of Tulsona Creek DBT Girder

Table 5-3. Selected Parameters in Tulsona DBT Girder

Parameter	Value	Remark
unit weight of concrete	$\gamma_c = 153 pcf$	concrete mix document
Concrete compressive strength	$f_c^{'} = 7500 psi$	specified 28day strength
	$f_{ci}^{'} = 6250 psi$	at force transfer
Elastic modulus	$E_{ci} = 5143000 psi$	at force transfer
Relative humidity	*RH=0.7*	AASHTO LRFD
Volume-surface ratio	*3.72 in.*	DBT girder

Table 5-4 shows the sum of time-dependent pre-stress losses estimated from the three methods. The value from the 2004 AASHTO method is close to the value from the 2017 AASHTO method. The 2017 AASHTO method with ACI 209-92 creep coefficients estimates a larger loss.

Table 5-4. Comparison of Pre-Stress Loss Due to Concrete Creep in Tulsona DBT Girder

Method	**0 – Bridge Completion**	**- 75 years**	**Total**
2004 AASHTO	NA	NA	29.8 ksi
2017 AASHTO	16.2 ksi	9.74 ksi	25.9 ksi
2017 AASHTO + ACI Creep Coeff.	20.3 ksi	15.9 ksi	36.2 ksi

CHAPTER. 6 SUMMARY AND CONCLUSIONS

6.1 Summary

Accurate estimation of pre-stress losses is an important issue for the design of precast, pre-stressed concrete bridge girders. If the pre-stress losses are underestimated, the concrete at the midspan of a girder may experience tensile stresses that exceed the cracking strength of the concrete, which can significantly compromise the durability and long-term performance of the girder. If the pre-stress losses are overestimated, however, more pre-stressing strands will be required than are necessary, which may increase the cost of girder fabrication, reduce the maximum span length, or increase the number of girders. Many researchers have studied this subject; however, data for pre-stress losses in cold climates are minimal. In the present research, long-term pre-stress loss due to concrete creep is studied based on a concrete creep test.

The project fabricated two concrete creep test frames, and one installed in the structural engineering laboratory at University of Alaska Fairbanks (UAF). The other frame was located outside a building on the UAF campus under ambient environment conditions. In each of the test frames, two 6″×12″ cylindrical specimens were loaded up to 33% of the 14-day compressive strength. The project used additional unloaded specimens, made from the concrete mix used for the fabrication of actual DBT girders, placed next to each frame for measuring concrete shrinkage strain. Specimens were made from the concrete mix used for a fabrication of actual DBT girders. Demountable Mechanical Strain Gauge (DEMEC) measured the concrete strains, and the thermistor embedded in cylinders measured specimen internal temperature. The concrete strains were collected for 11 months (7/26/2017 – 6/21/2018) after loading.

During the period of measurement, the outdoor ambient temperature dropped below 0°C between 100 and 250 days after measurement started. The project observed the following in concrete strain measurement.

- Between 0 and 50 days after measurement started, the total strains from the outdoor frame were greater than the ones from the indoor frame. Between 50 and 100 days after measurement started, two curves from the two frames are similar in their patterns and values. After 100 days, the total strain from the indoor frame slowly increased reaching between 1,600 and 1,700 $\mu\varepsilon$ after 250 days. However, the total strain from the outdoor frame varied between 1,000 and 1,500 $\mu\varepsilon$ and the averaged total strain was 1,300 $\mu\varepsilon$ after 250 days.
- The shrinkage strain from indoor specimens showed a change of roughly 500$\mu\varepsilon$ in the first 50 days, then a steadily increasing trend until measurements stop to a maximum of 1,000$\mu\varepsilon$. The outdoor specimens showed a similar trend within the first 50 days at roughly 500$\mu\varepsilon$. Between 150 and 250 days after measurement started, the strain did not change much compared to the indoor specimens.
- Comparing the four creep and shrinkage models in ACI 209.2R-08 (ACI 2008) and the one in the AASHTO LRFD (AASHTO 2017), the measured total strains from the indoor frame matched well with the CEB MC90-99 model. The measured total strains from the outdoor frame matched well with the ACI 209-92 model.
- The time-dependent pre-stress losses were predicted based on the 2017 AASHTO LRFD Refined method where the creep coefficients and shrinkage were modified

following the ACI 209-92 model. The estimated losses were greater than the ones from the 2004 AASHTO LRFD method and the 2017 AASHTO LRFD method.

6.2 Conclusion

Bridge construction in Alaska occurs mostly in the summer season and evidence shows that the majority of the concrete creep takes place within the first 6 months of placement; the winter season should have minimal effects on the short-term creep. However, the wildly fluctuating winter's cold and summer heat may have more of an effect on the long-term creep. The prediction models are not able to predict accurately this long-term creep as the relative humidity and temperature are constantly shifting.

The project observed that the natural environment including the ambient air temperature and relative humidity is a big factor in the extent of creep and shrinkage. This fact is displayed in the differences of ambient versus internal temperature of the outdoor apparatus. Figure 4-35 shows that after roughly 80-100 days when the ambient temperature reaches zero degrees, the creep almost stops. This is evidence that the ambient temperature relates directly to the amount of shrinkage and creep within the concrete specimens. Thus, for areas represented by the parameters of the indoor specimen, the ACI 209R-92 or the CEB MC 90-99 models may be the best selection based on the 1-year prediction from Figure 5-3. Whereas areas that are more prone to big variations in temperature and relative humidity may want to refer to the predictions representing the ambient environment for predicting pre-stress loss.

In the cold climate, the concrete creep and shrinkage can occur for a longer period since cold temperature suppresses creep and shrinkage. When implementing long-term monitoring for

creep and shrinkage strains in a cold climate, the period and frequency of strain measurement should be determined based on seasonal ambient temperature changes.

6.3 Future Studies

The future work done regarding concrete shrinkage and creep needs more control over the ambient temperatures to get quantifiable results of their differences similar to the model predictions. This can be accomplished by placing an apparatus in a cold room where the temperature and relative humidity are maintained throughout the experiment. In addition, the number of specimens utilized for this experiment were few and to obtain a more accurate representation of the values more frames and more locations are required.

REFERENCES

AASHTO (2004). *AASHTO LRFD Bridge Design Specifications (3rd ed.),* American Association of State Highway and Transportation Officials.

AASHTO (2012). *AASHTO LRFD Bridge Design Specifications (6th ed.),* American Association of State Highway and Transportation Officials.

AASHTO (2014). *AASHTO LRFD Bridge Design Specifications (7th ed.),* American Association of State Highway and Transportation Officials.

AASHTO (2017). *AASHTO LRFD Bridge Design Specifications (8th ed.),* American Association of State Highway and Transportation Officials.

ACI (1992). *Prediction of Creep, Shrinkage, and Temperature Effects in Concrete Structures (ACI 209R-92).* American Concrete Institute, Farmington Hills, MI. 47 pp.

ACI (2005). *Report on Factors Affecting Shrinkage and Creep of Hardened Concrete (ACI 209.1R-05).* American Concrete Institute.

ACI (2008). *Guide for Modeling and Calculating Shrinkage and Creep in Hardened Concrete (ACI 209.2R-08).* American Concrete Institute.

ADOT&PF (2017). *Alaska Bridges and Structures Manual*. Alaska Department of Transportation and Public Facilities.

Aguilar, C. (2005). *Study of the Behavior and Development of a Prediction Methodology for Drying Shrinkage of Concretes*. PhD thesis. School of Engineering, Universidad Catolica de Chile, Santiago, Chile.

ASTM (2012). *Standard Practice for Making and Curing Concrete Test Specimens in the Field (ASTM C31 / C31M-12).* ASTM International

ASTM (2014). *Standard Test Method for Static Modulus of Elasticity and Poisson's Ratio of Concrete in Compression (ASTM C469 / C469M – 14).* ASTM International.

ASTM (2015). *Standard Test Method for Creep of Concrete in Compression (C 512/C512M-15).* ASTM International.

ASTM (2018). *C39 / C39M-18, Standard Test Method for Compressive Strength of Cylindrical Concrete Specimens*. ASTM International, West Conshohocken, PA.

Bažant, Z.P. (1987). Statistical Extrapolation of Shrinkage Data – Part I: Regression. *ACI Materials Journal* 84(1):20-34.

Bažant, Z. P. (2000). Criteria for Rational Prediction of Creep and Shrinkage of Concrete. *The Adam Neville Symposium: Creep and Shrinkage-Structural Design Effects, SP-194,* A. Al-Manaseer, ed.:237-260. American Concrete Institute, Farmington Hills, MI.

Bažant, Z.P., and S. Baweja (1995). Creep and Shrinkage Prediction Model for Analysis and Design of Concrete Structures – Model B3. *Materials and Structures* 28:357-365, 415-430, 488-495.

Bažant, Z. P., and S. Baweja (2000). Creep and Shrinkage Prediction Model for Analysis and Design of Concrete Structures: Model B3. *The Adam Neville Symposium: Creep and Shrinkage-Structural Design Effects, SP-194,* A. Al-Manaseer, ed.: 1-83. American Concrete Institute, Farmington Hills, MI.

Brewe, J. E., J. J. Myers and J. Myers (2008). Pre-stress Loss Behavior of High-Strength Self-Consolidating Concrete Girders Subjected to Elevated Compressive Fiber Stresses. *National Bridge Conference*.

CEB (1999). Structural Concrete—Textbook on Behaviour, Design and Performance. Updated Knowledge of the CEB/ FIP Model Code 1990. *fib Bulletin 2*, 2: 37-52. Federation Internationale du Beton, Lausanne, Switzerland.

ClimaTemps (2016). *Climate & Temperature*. http://www.climatemps.com/.

Collins, M. P. and D. Mitchell (1997). *Pre-stressed Concrete Structures*. Response Publications.

Current Results Nexus (2016a). *Humidity Levels in Montana During January*. https://www.currentresults.com/ /Montana/humidity-january.php.

Current Results Nexus (2016b). *Winter Temperature Averages for Every State*. https://www.currentresults.com/Weather/US/average-state-temperatures-in-winter.php.

Daugherty, L. and E. Marx (2014). ALASKA Concrete bridges in extreme and remote environments. *ASPIRE* (Summer):34-35.

Figg, L. and W. D. Pate (2004). Precast Concrete Segmental Bridges-America's Beautiful and Affordable Icons. *PCI Journal* 49(5):26-38.

Garber, D. B., J. M. Gallardo, D. J. Deschenes and O. Bayrak (2016). Pre-stress loss calculations: Another perspective. *PCI Journal*(May-June):68-85.

Garber, D., J. Gallardo, D. Deschenes, D. Dunkman and O. Bayrak (2013). *Effect of New Pre-stress Loss Estimates on Pre-tensioned Concrete Bridge Girder Design (FHWA/TX-12/0-6374-2)*. Center for Transportation Research, The University of Texas at Austin; Texas Department of Transportation.

Gardner, N. J., and J. J. Lockman (2001). Design Provisions for Drying Shrinkage and Creep of Normal Strength Concrete. *ACI Materials Journal* 98(2):159-167. Mar.-Apr.

Josten, M. G., W. L. Painter and J. S. Guarre (1995). Precast Pre-stressed Concrete Structure Provides Solution for Getty. *PCI Journal* 40(3):24-39.

Menn, C. (1986). *Pre-stressed Concrete Bridges*, Birkhauser.

Mertol, H. C., S. Rizkalla, P. Zia, and A. Mirmiran (2010). Creep and shrinkage behavior of high-strength concrete and minimum reinforcement ratio for bridge columns. *PCI Journal*(summer):138-154.

Muller, H. S., and H. K. Hilsdorf (1990). *General Task Group 9*. CEB Comité Euro-International du Béton, Paris, France.

Oesterle, R. G., A. F. Elremaily, Z. J. Ma, R. Eriksson and C. Prussack (2009). *Design and Construction Guidelines for Long-Span Decked Precast, Pre-stressed Concrete Girder Bridges (Final Report, NCHRP Project 12-69)*. National Cooperative Highway Research Program; Transportation Research Board.

Park, R. and T. Paulay (1975). *Reinforced Concrete Structures*. John Wiley and Sons.

PCI (2000). *Precast Pre-stressed Concrete Bridge Design Manual*. Precast/Pre-stressed Concrete Institute. Chicago, IL.

PCI (2010). *PCI Design Handbook: Precast and Pre-stressed Concrete. MNL-120 (7th ed.)*. Precast/Pre-stressed Concrete Institute. Chicago, IL.

PCI (2011). *Chapter 6. Preliminary Design. Bridge Design Manual (3rd Ed.)*. Precast/Pre-stressed Concrete Institute. Chicago, IL.

PCINE (2014). *Guidelines for Accelerated Bridge Construction Using Precast/Pre-stressed Concrete Elements Including Guideline Details (2nd ed., PCINE-14-ABC)*. Precast/Pre-stressed Concrete Institute Northeast Bridge Technical Committee.

Roller, J. J., H. G. Russell, R. N. Bruce and W. R. Alaywan (2011). Evaluation of pre-stress losses in high-strength concrete bulb-tee girders for the Rigolets Pass Bridge. *PCI Journal* 56(1):110-134.

Rüsch, H. (1960). Researches Toward a General Flexural Theory for Structural Concrete. *ACI-Journal Proceedings* 57(7):1-28.

Shahawy, M. A. (2003). *Prefabricated Bridge Elements and Systems to Limit Traffic Disruption During Construction (NCHRP Synthesis 324)*. Transportation Research Board.

Tadros, M. K., N. Al-Omashi, S. J. Seguirant and J. G. Gallt (2003). Pre-stress Losses in Pre-tensioned High-Strength Concrete Bridge Girders (NCHRP Report 496). Washington, D.C., Transportation Research Board.

Wikipedia. (2016a). *Helena, Montana*. https://en.wikipedia.org/wiki/Helena,_Montana.

Wikipedia. (2016b). *Spokane, Washington*. https://en.wikipedia.org/wiki/Spokane,_Washington.

APPENDIX **A**

Appendix A: Submitted and Approved Girder Design

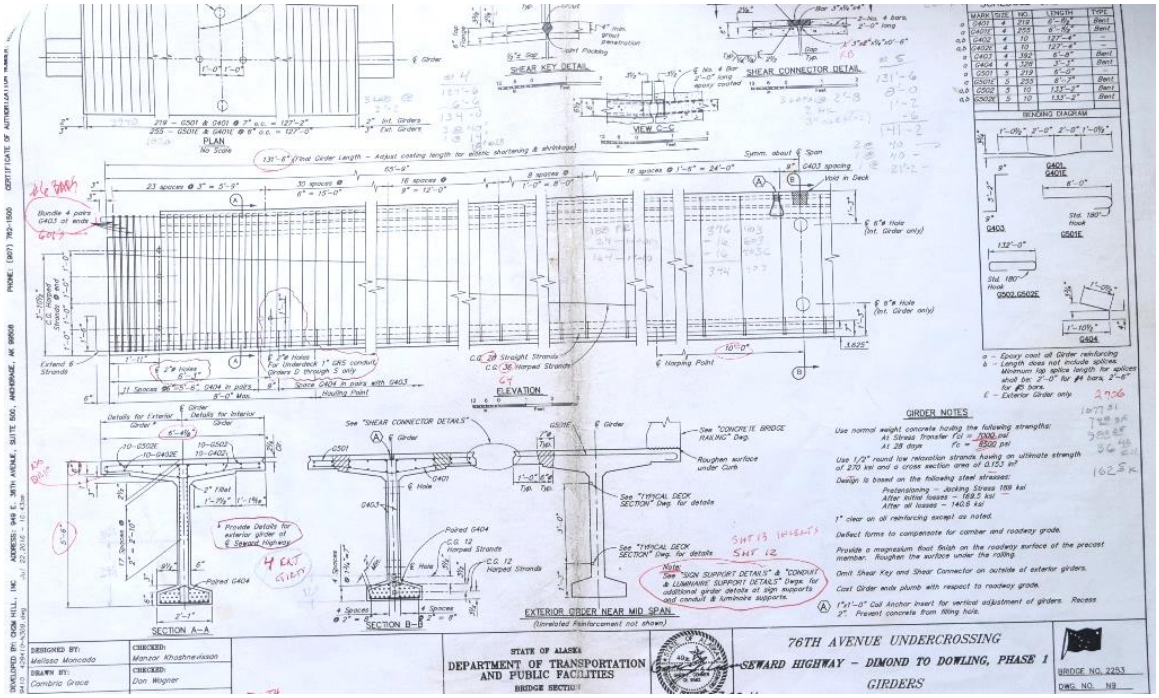

APPENDIX B: MEASURED DATA

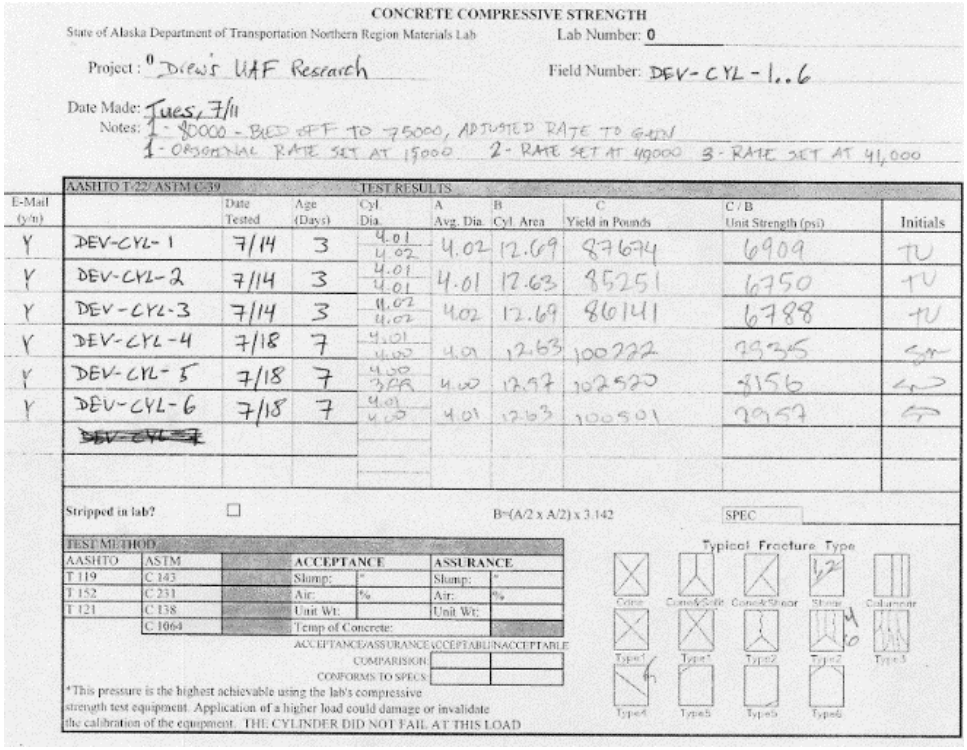

CONCRETE COMPRESSIVE STRENGTH

State of Alaska Department of Transportation Northern Region Materials Lab — Lab Number: 0

Project: 0 Drew's UAF Research — Field Number: DEV-CYL-1..6

Date Made: Tues, 7/11

Notes: 1- 80000 - BLED OFF TO 75000, ADJUSTED RATE TO 6KN
1- ORIGINAL RATE SET AT 15000 2- RATE SET AT 40000 3- RATE SET AT 41,000

AASHTO T-22/ ASTM C-39 — TEST RESULTS

E-Mail (y/n)		Date Tested	Age (Days)	Cyl. Dia.	A Avg. Dia.	B Cyl. Area	C Yield in Pounds	C / B Unit Strength (psi)	Initials
Y	DEV-CYL-1	7/14	3	4.01 4.02	4.02	12.69	87674	6909	TV
Y	DEV-CYL-2	7/14	3	4.01 4.01	4.01	12.63	85251	6750	TV
Y	DEV-CYL-3	7/14	3	4.02 4.02	4.02	12.69	86141	6788	TV
Y	DEV-CYL-4	7/18	7	4.01 4.02	4.01	12.63	100222	7935	
Y	DEV-CYL-5	7/18	7	4.00 3PA	4.00	12.97	102520	8156	
Y	DEV-CYL-6	7/18	7	4.01 4.00	4.01	12.63	100501	7957	
	~~DEV-CYL-7~~								

Stripped in lab? ☐ B=(A/2 x A/2) x 3.142 SPEC

TEST METHOD

AASHTO	ASTM	ACCEPTANCE		ASSURANCE	
T 119	C 143	Slump:	"	Slump:	"
T 152	C 231	Air:	%	Air:	%
T 121	C 138	Unit Wt:		Unit Wt:	
	C 1064	Temp of Concrete:			

ACCEPTANCE/ASSURANCE ACCEPTABLE/UNACCEPTABLE
COMPARISION
CONFORMS TO SPECS

*This pressure is the highest achievable using the lab's compressive strength test equipment. Application of a higher load could damage or invalidate the calibration of the equipment. THE CYLINDER DID NOT FAIL AT THIS LOAD

Typical Fracture Type

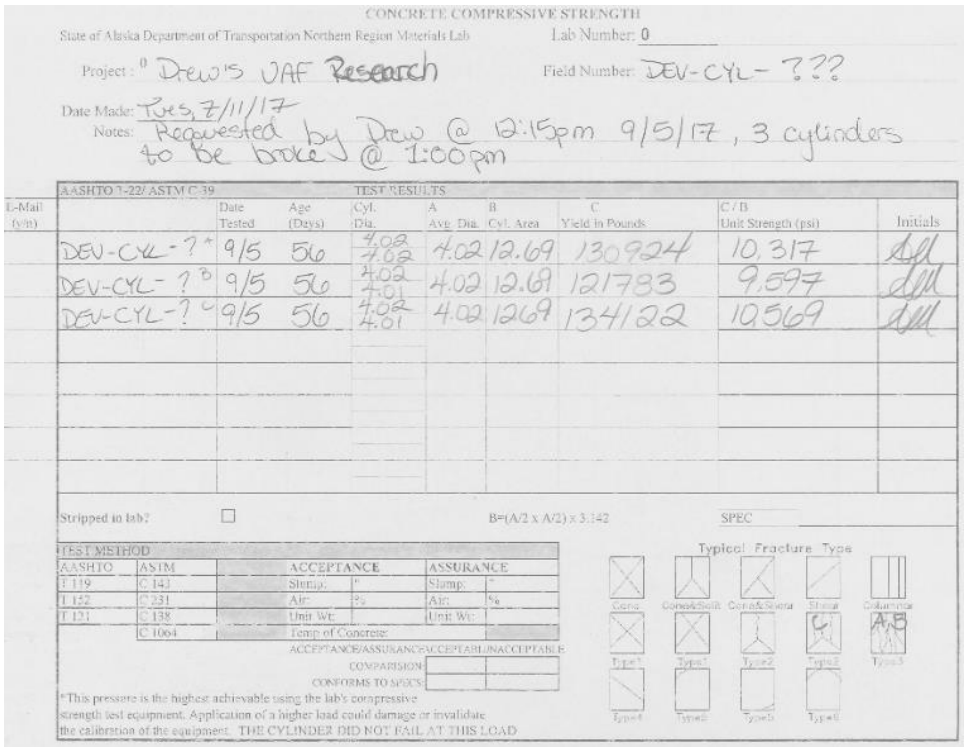

CONCRETE COMPRESSIVE STRENGTH

State of Alaska Department of Transportation Northern Region Materials Lab — Lab Number: 0

Project: 0 Drew's UAF Research — Field Number: DEV-CYL-???

Date Made: Tues, 7/11/17

Notes: Requested by Drew @ 12:15pm 9/5/17, 3 cylinders to be broke @ 1:00pm

AASHTO T-22/ ASTM C-39 — TEST RESULTS

E-Mail (y/n)		Date Tested	Age (Days)	Cyl. Dia.	A Avg. Dia.	B Cyl. Area	C Yield in Pounds	C / B Unit Strength (psi)	Initials
	DEV-CYL-?*	9/5	56	4.02 4.02	4.02	12.69	130924	10,317	dm
	DEV-CYL-?°	9/5	56	4.02 4.01	4.02	12.61	121783	9,597	dm
	DEV-CYL-?^	9/5	56	4.02 4.01	4.02	1269	134122	10569	dm

Stripped in lab? ☐ B=(A/2 x A/2) x 3.142 SPEC

TEST METHOD

AASHTO	ASTM	ACCEPTANCE		ASSURANCE	
T 119	C 143	Slump:	"	Slump:	"
T 152	C 231	Air:	%	Air:	%
T 121	C 138	Unit Wt:		Unit Wt:	
	C 1064	Temp of Concrete:			

ACCEPTANCE/ASSURANCE ACCEPTABLE/UNACCEPTABLE
COMPARISION
CONFORMS TO SPECS

*This pressure is the highest achievable using the lab's compressive strength test equipment. Application of a higher load could damage or invalidate the calibration of the equipment. THE CYLINDER DID NOT FAIL AT THIS LOAD

Typical Fracture Type

CONCRETE COMPRESSIVE STRENGTH

State of Alaska Department of Transportation Northern Region Materials Lab — Lab Number: 0

Project: 0 Drew's UAF Research — Field Number: DEV-CYL-7..12

Date Made: Tues, 7/11

Notes: Cyl 10- Rate set at 80000 - stalled at 115k, required adjustment to rate of 200
Cyl 11- Rate set at 87,000 - stalled at 103k, required adjustment to rate of 200
Cyl 12- Rate set at 87,000 - didn't stall

AASHTO T-22/ ASTM C-39 — TEST RESULTS

E-Mail (y/n)		Date Tested	Age (Days)	Cyl. Dia.	A Avg. Dia.	B Cyl. Area	C Yield in Pounds	C / B Unit Strength (psi)	Initials
Y	DEV-CYL-7	8/8	28	4.03 4.02	4.02	12.69	121939	9609	CS
Y	DEV-CYL-8	8/8	28	4.01 4.02	4.02	12.69	116818	9206	CS
Y	DEV-CYL-9	8/8	28	4.02 4.02	4.02	12.69	108406	8543	CS
Y	DEV-CYL-10	10/9	90	4.01 4.02	4.02	12.69	124937	9845	TV
Y	DEV-CYL-11	10/9	90	4.02 4.02	4.02	12.69	125978	9927	TV
Y	DEV-CYL-12	10/9	90	4.01 4.01	4.01	12.63	123317	9764	TV

Stripped in lab? ☐ — B=(A/2 x A/2) x 3.142 — SPEC

TEST METHOD			ACCEPTANCE		ASSURANCE	
AASHTO	ASTM		Slump:	"	Slump:	"
T 119	C 143		Air:	%	Air:	%
T 152	C 231		Unit Wt:		Unit Wt:	
T 121	C 138		Temp of Concrete:			
	C 1064					

ACCEPTANCE/ASSURANCE\ACCEPTABLE/UNACCEPTABLE

COMPARISION

CONFORMS TO SPECS

*This pressure is the highest achievable using the lab's compressive strength test equipment. Application of a higher load could damage or invalidate the calibration of the equipment. THE CYLINDER DID NOT FAIL AT THIS LOAD

Typical Fracture Type

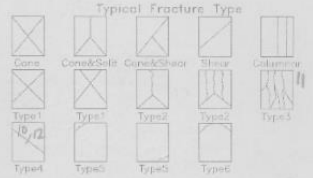

DOWL HKM

☑ CONCRETE ☐ MORTAR ☐ GROUT

Dispatch Date: 7-11-17
Dispatch Time: 1:30
Page 1 of 1

Client: ADOT 3 PF		Project Number: AK 35001
Project: SR Dewatering to Dowling		Contractor: Oop
Order Taken By: EJ	Order Requested By: Geoff Jackson	Date/Time Requested: 7-11-17
Test Locations Selected By: ☑ ATL ☐ Contractor ☐ Owner		
Notification of Test Results Given To (Date and Time):		
Time Dispatched to Site: 1:30	Time Arrived at Site: 1:45	Tested by/Date: EJ 7-11-17
Time Dispatched Site: 0:30	Time Arrived Back: 3:45	Reviewed by/Date:
Specification:		
Supplier: Aggpro	Product Code: 1740 Class P	Pour Volume: 37.25 yd³
Slump: 9" max	Air: 3±1.5	Strength: 8500 @ 28 days W/C: Unit Wt:

Today's Set No	1				Location
Total Air	—				Girder 225-G
Aggregate Correction	—				
Entrained Air	2.5 %				
Slump	9 "				
Unit Weight	152.2				
Concrete Temperature	64 °				
Pour Air Temperature	57 °				
Σ yd³ Poured	3 F 37.25				
Ticket No	30124351				
Size/No. Specimens	6-4x8				

REMARKS

3-1 FC
3-28 d

Jan Calhoun
Wagtech 1111
38.04/0.25

7000 psi required for detension

☐ Unit Price ☐ T&M

Cylinders Picked Up by/date:	Site Visit:	Min/Max Temperature:

Tested by date: